Vulnerability Assessment and Reduction for Intermodal Freight Transportation Networks

Xiaoyang Wei [a,b], *Mengtong Wang* [b], *Qiang Meng* [b*]

[a] *Institute of High Performance Computing, Agency for Science, Technology and Research (A*STAR), Singapore 138632*

[b] *Department of Civil and Environmental Engineering, National University of Singapore, Singapore 117576*

Abstract

Intermodal freight transportation networks (IFTNs) are critical for global logistics, facilitating the efficient transportation of cargo within containers by integrating diverse transportation modes. However, such integration exposes IFTNs to a variety of disruptions, may leading to degradation in transportation capabilities. Thus, vulnerability assessment and reduction (VA&R) for IFTNs are of practical significance. Despite its importance, this research problem has received little attention in the literature. To fill the research gap, we propose the VA&R problem for IFTNs, considering uncertain disruptions that impact IFTN nodes and links, along with cascading failures and influence spreading. We further build models incorporating two-stage robust optimization to assess and reduce the impact of uncertain disruptions, and build exact solution methods for VA&R utilizing column-and-constraint generation and speedup strategies to identify non-conservative solutions. The effectiveness and efficiency of our modeling and solution methods are demonstrated by comparing them to benchmark modeling and solution methods, through numerical experiments for a real-world international IFTN. Furthermore, managerial insights and recommendations for IFTN operations are achieved based on comprehensive sensitivity analyses to address uncertain disruptions in IFTNs.

Keywords: Intermodal freight transportation network; Vulnerability assessment; Vulnerability reduction; Max-min optimization; Two-stage robust optimization; Column-and-constraint generation.

[*] Corresponding author (Q. Meng). E-mail: ceemq@nus.edu.sg, Tel.: +65 6516 5494.

1. Introduction

Intermodal freight transportation networks (IFTNs) play a vital role in global freight transportation, offering economical, efficient, and safe cargo movement by synergizing various transportation modes [1]. However, the intricately connected nature of IFTNs exposes them to a variety of uncertain disruptions, such as public health emergencies, natural disasters, and unforeseen accidents. These disruptions are characterized by several uncertain factors: (i) occurrence locations that are usually unpredictable, (ii) multiplicity ranging from rare to widespread, (iii) severity levels varying from facility intact to complete-failure, (iv) impact scopes spaning from localized to network-wide, (v) timing that may coincide with peak transportation periods, and so on. Meanwhile, the just-in-time principle allows little flexibility to adjust freight transportation and exacerbates the impact of disruptions. Consequently, these disruptions can compromise the functionality of transportation facilities, resulting in reduced capabilities or even complete closures, thereby revealing the vulnerabilities of IFTNs. Therefore, vulnerability assessment and reduction (VA&R) for IFTNs have become a significant concern to maintain IFTN performance.

Despite the importance of VA&R for IFTNs, existing research primarily focuses on IFTN performance in disruption-free situations [2], with limited literature addressing VA&R for IFTNs, particularly regarding (i) disruptions with uncertainty, (ii) complete or partial failures in nodes and links (including intermodal links that connect different transportation modes), and (iii) cascading failures and influence spreading within IFTNs. To address the research gap, this study is the first to simultaneously consider all the above three aspects for already-constructed IFTNs, by building robust optimization modeling and solution methods of VA&R. Particularly, we deal with disruption uncertainty by examining multiple aspects: (i) the unpredictability of occurrence locations and multiplicity using multiple budgeted uncertainty sets, (ii) the severity levels which range from partial to complete failures, (iii) the impact scopes that includes the potential for cascading failures and influence spreading, and (iv) the timing which we analyze by adjusting demand volumes to account for peak and non-peak transportation periods. Accordingly, we build a two-stage robust optimization method for already-constructed IFTNs that characterizes unpredictable disruptions using budgeted uncertainty sets, circumventing the need for precise probability information which is challenging to calibrate for certain disruptions, such as the Suez Canal blockage. Furthermore, this method overcomes the limitation of static robust optimization, which may result in over-conservative solutions, because static robust optimization lacks recourse actions in a second-stage decision-making process for realized uncertain disruptions. In a nutshell, our modeling and solution methods aid decision-makers in effectively assessing and reducing vulnerabilities for IFTNs, particularly in the context of uncertain disruptions.

1.1. Research scope

The vulnerability in transportation systems has a variety of definitions, and readers may refer to [3–5] for a range of interpretations of this concept. Following an extensive literature survey, this study defines *vulnerability* as the susceptibility to disruption events that result in a degradation in the network capability. Vulnerability is measured by the increment in transit costs and penalty costs for unmet demand given the occurrence of disruptions. To clarify the concept of vulnerability and delineate the research scope, we present a schematic illustration of capability evolution for the IFTN in Figure 1. The required capability level P_0 is indicated by a bold black line, while the daily fluctuation of capability is depicted by a wavy line surrounding the bold black line. Disruptions, such as the Suez Canal blockage event in March 2021, cause a degradation in the network capability until it reaches the worst capability at time t_d, after which the network capability may recover to the normal level at time t_r. *Vulnerability* is measured by $P_0 - P(t_d)$, namely, the decrease in network capability under disruptions. It is noteworthy that *robustness*, the remained capability in the worst situation under disruptions (i.e., $P(t_d)$ in Figure 1), is regarded as the inverse concept of vulnerability [6]. The scope of this research is to assess and reduce vulnerability of IFTNs, because the concept of vulnerability offers a more direct view on the impact of disruptions in IFTNs. It is evident that a network exhibiting less vulnerability will possess higher robustness, and vice versa.

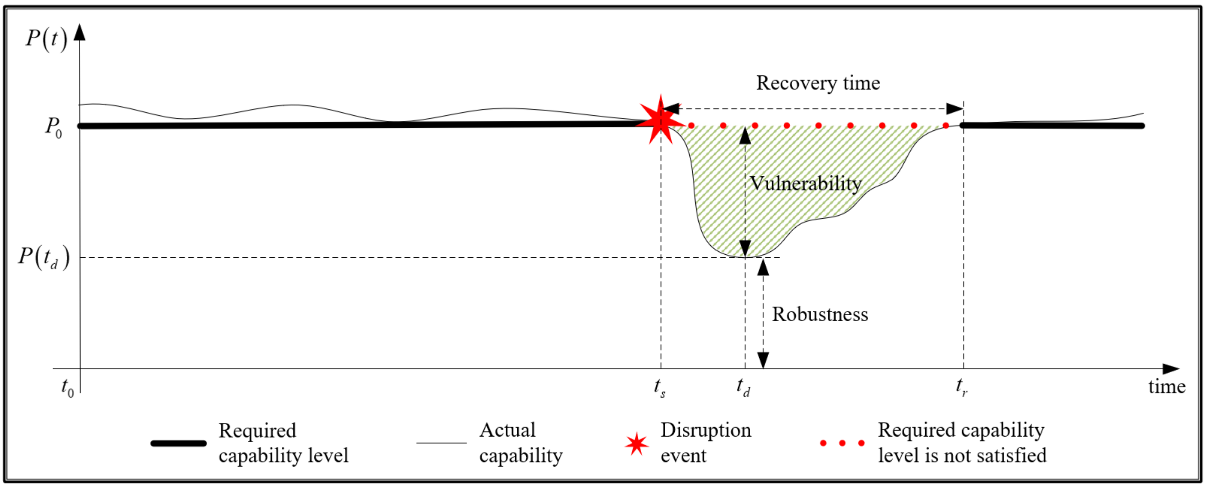

Figure 1. The schematic capability of an IFTN.

To implement VA&R for the IFTN, a *disruption* is defined as the failure of a single node (e.g., a train station) or link (e.g., a railway between two train stations) in the IFTN, resulting in a degradation in the capacity of the corresponding node or link. A *disruptive scenario* refers to a situation where the IFTN experiences multiple disruptions. Under a disruptive scenario, some freight transportation may necessitate rescheduling or cancellation. Correspondingly, *vulnerability assessment* is based on two aspects: (i) the increment in transit costs and (ii) the penalty costs for unmet demand incurred by the disruptive scenario. *Vulnerability reduction* can be achieved by (i) identifying the vulnerable and key network nodes and links and (ii) implementing proactive maintenance at an appropriate level for the identified nodes and links. For example, waterway maintenance can efficiently reduce the probability and impact of disruptions caused by ship accidents [7].

1.2. Contributions

The main contributions of this study are three-fold.

(i) To the best of our knowledge, this is the first work to investigate VA&R for already-constructed IFTNs amid uncertain disruptions in both nodes and links, explicitly including intermodal links that connect different transportation modes. Moreover, this study considers cascading failures and influence spreading, realistically capturing the inherent interconnection and interdependence features of IFTNs.

(ii) For the first time, the VA&R for already-constructed IFTNs is addressed by a two-stage robust optimization method, incorporating single and multiple uncertainty sets, and accounting for partial and complete failures of network elements. The utilization of budgeted uncertainty sets circumvents the need for exact probability information, which is usually difficult to ascertain for certain disruptions. The two-stage robust optimization method addresses the shortcomings of static robust optimization techniques, by mitigating the tendency towards overly conservative solutions. Moreover, a tailored exact algorithm that combines column-and-constraint generation (C&CG) with speedup strategies is introduced, calculating optimal solutions for the already-constructed IFTN, with demonstrable superiority over the benchmark algorithm - Benders decomposition (BD).

(iii) This study offers crucial managerial insights and strategic recommendations for managing disruptions during the IFTN operations, underpinned by extensive numerical experiments and sensitivity analyses for a real-world IFTN. Meanwhile, the results underscore the efficacy of the developed modeling and solution methods in significantly reducing network vulnerability at small maintenance costs. Additionally, these methods have potential applicability to other diverse freight transportation networks (including single-modal and multimodal networks) for VA&R purposes.

The remainder of this paper is organized as follows. Section 2 reviews the literature related to VA&R for IFTNs and identifies the research gaps. Section 3 elaborates on the VA&R problem arising from the IFTN operations. In Section 4, VA&R models are formulated and compared. In Section 5, the exact solution method incorporating C&CG and speedup strategies is developed. Section 6 provides details on instance generation, the benchmark algorithm, solution performance, and sensitivity analysis. Section 7 concludes this work and suggests directions for future research. For ease of presentation, the deterministic model (DM) for freight transportation in IFTNs under disruption-free conditions is presented in Appendix A, and the stochastic programming-based (SP-based) VA&R models are reported in Appendix B.

2. Literature Review and Research Gaps

This section presents a summarized literature review on VA&R for transportation networks. First, vulnerability assessment metrics and methods for transportation networks are examined. Next, vulnerability reduction methods for transportation networks are investigated. Finally, the research gaps are identified, and the novelty of our work is thus highlighted.

2.1. Vulnerability assessment

The studies [3,4] provide comprehensive and insightful overviews of transportation network vulnerability. Meanwhile, these studies reveal a gap in existing research on IFTNs and vulnerability reduction. Drawing on the literature, including [8], our study identifies representative vulnerability assessment metrics for transportation networks, as listed in the last column of Table 1.

Table 1. Representative work on vulnerability study for transportation networks.

Literature	Modal	Transportation modes included	VA&R	Disrupted elements	Disruption uncertainty	Complete or partial failures	Vulnerability assessment metric
Chen et al. (2002)[9]	Single	Road	Only assess	Only links	Yes	Both	Capacity reduction
Scott et al. (2006)[10]	Single	Freeway	Only assess	Only links	No	Only complete	Increment in transit time
Murray et al. (2007)[11]	Single	Generic network	Only assess	Only nodes	No	Only complete	Interdicted flow
Peterson and Church (2008)[12]	Single	Railway	Only assess	Only links	No	Only complete	Additional impedance and distance
Santos et al. (2010)[13]	Single	Road	Both	Only links	No	Only complete	Increment in transit cost
Sullivan et al. (2010)[14]	Single	Road	Only assess	Only links	No	Both	Total transit time
Jenelius and Mattsson (2012)[15]	Single	Road	Only assess	Only links	Yes	Only complete	Unsatisfied travel demand and delays
Gedik et al. (2014)[16]	Single	Railway	Only assess	Only nodes	No	Only complete	Operation cost and delay
Rodríguez-Núñez et al. (2014)[17]	Single	Metro	Only assess	Only links	No	Only complete	Total transit time
Khaled et al. (2015)[18]	Single	Railway	Only assess	Only nodes or links	No	Only complete	Generalized total cost
Stamos et al. (2015)[19]	Multimodal (for passengers)	Road, railway, and air	Only assess	Only intermodal links among transportation modes	No	Only complete	Transit time and monetary cost
Wang et al. (2016)[20]	Single	Road	Only assess	Only links	No	Only complete	Maximum transit time
Bell et al (2017)[21]	Single	Road	Only assess	(No consideration of disruptions)	N.A.	N.A.	Minimum-capacity bottleneck
Cats et al. (2017)[22]	Multimodal (for passengers)	Metro and tram	Only assess	Only links (excluding intermodal links among modes)	No	Both	Total transit cost
Darayi et al. (2017)[23]	Intermodal	Freeway, railway, and waterway	Only assess	Nodes and links (excluding intermodal links among modes)	No	Both	Sum of specific commodity flows
Whitman et al. (2017)[24]	Single	Railway	Only assess	Only links	No	Only complete	Unmet demand
Zhou and Wang (2018)[25]	Single	Freeway	Only assess	Only links	No	Only complete	Total transit time
Szymula and Bešinović (2020)[26]	Single	Railway	Only assess	Only links	No	Only complete	Disconnected passengers and passenger detours
He et al. (2021)[27]	Multimodal (for freight)	Road, railway, and river	Only assess	Only links	No	Both	Increment in transit time
Lu et al. (2022)[28]	Single	Railway	Only assess	Only nodes	No	Only complete	No. of failed nodes and impacts on passengers
Wen et al. (2022)[29]	Single	Sea or other mode	Only assess	Only nodes	Yes	Only complete	Network centrality
Zhang et al. (2024)[30]	Single	Railway	Only assess	Only nodes	No	Only complete	Ratio of residual flow
Wen et al. (2024)[31]	Single	Road	Both	Only links	No	Only complete	Change in connectivity efficiency
This work	**Intermodal**	**Road, railway, river, and sea**	**Both**	**Nodes and links (including intermodal links among modes)**	**Yes**	**Both**	**Increment in transit costs and penalty costs**

Vulnerability assessment methods are typically classified into three categories.

(i) *Topological methods.* They utilize metrics based on complex network and graphical theory [32]. Such methods track the evolution of network capability by removing nodes or links to assess network vulnerability [33]. Though topological methods are capable of identifying key network elements through complete enumeration, they are associated with a prohibitively high computational burden when applied to large networks with multiple element removals [34].

(ii) *Simulation methods.* They are similar to topological methods, but assess vulnerability in dynamic and stochastic ways by simulation [35]. These methods simulate disruptive scenarios, which can be time-consuming for high-resolution models, and require the consideration of an exponential number of network element combinations [36].

(iii) *Optimization methods.* They are applicable to transportation network modeling, and thus can identify the worst disruptive scenario without enumerating all possible scenarios. Representative examples of optimization methods include interdiction methods for studying multi-element failures in railway networks [16], single-element removal procedures for assessing the vulnerability of railway networks [18], transit assignment methods based on equilibrium and flow-dependent transit time for identifying the worst disruptive scenario [20], multi-commodity-flow models with single-element removal methods for assessing vulnerability for multiple commodities [24], and heuristic algorithms for identifying the most critical multi-link blockage with considering capacity limits and congestion influence [37]. Notably, optimization methods often lead to extensive computational requirements, particularly for complex and large-scale networks.

2.2. Vulnerability reduction

The literature on vulnerability reduction shows that probability-based methods are frequently used to address disruptions in transportation systems [38,39]. However, these methods encounter challenges in calibrating the probability of disruption events due to limited historical data. For example, calibrating the accurate probability of Suez Canal blockage is difficult. An alternative approach is to employ robust optimization, an optimization method designed to handle uncertainty [40]. Robust optimizations can characterize unpredictable disruptions by defining uncertainty sets, thereby eliminating the reliance on precise probability information. Nevertheless, the static robust optimization method may be overly conservative since it does not consider recourse actions for realized uncertainties. To address this issue, the two-stage robust optimization technique has been studied, which calculates recourse decisions (e.g., freight rescheduling after realized disruptions in transportation networks) following the first-stage decision and the revealed scenario [41]. Solving the two-stage robust optimization model poses significant challenges, and three categories of algorithms have been explored: (i) Approximation algorithms, which employ simplified functions to approximate the problem [42,43]; (ii) BD algorithms, which use the dual of the second-stage problem to derive the value function of the first-stage decision, but the computation time increases rapidly with the growth in instance size [44]; and (iii) C&CG algorithms, which have demonstrated efficiency in handling two-stage robust optimization, especially for designing yet-to-be-constructed transportation networks [45–48]. Following an exhaustive literature review, this work adopts the C&CG algorithm framework to build a two-stage robust optimization algorithm tailored for the VA&R of IFTNs.

2.3. Research gaps

Table 1 presents a summary of representative vulnerability research for transportation networks. Three studies are particularly relevant to this work, although each of them exhibits certain limitations. Chen et al. [9] consider both complete and partial failures, as well as disruption uncertainty. However, they use a conventional Monte Carlo method to simulate the uncertainty, which can be computationally intensive and may not accurately represent the true probability distributions of uncertain events. Moreover, the study focuses solely on vulnerability assessment without addressing vulnerability reduction. Santos et al. [13] analyze both assessment and reduction of vulnerability but ignore disruption uncertainty. This limitation constrains the practicality of the solution method and the real-world relevance of the problem. Furthermore, this study only considers small networks with single-modal transportation, rather than intermodal transportation. Although Darayi et al. [23] focus on IFTNs, they do not consider the intermodal links and transfer operations among different transportation modes. Moreover, this study does not consider disruption uncertainty or vulnerability reduction.

In addition, this work distinguishes itself from existing research on logistics or power network design, such as [47–49], which focus on facility location and capability planning to design yet-to-be-constructed networks. In contrast, our work investigates already-constructed IFTNs involving maintenance decisions. Specifically, our work differs from [47–49] in two main aspects:

(i) Studies [47] and [48] primarily explore methods for designing logistics networks resilient to disruptions. Their aims revolve around planning the optimal network structure and facility capacity.

However, our work focuses on already-constructed IFTNs (where facility location and capacity are given parameters), specifically assessing IFTN performance and devising maintenance decisions, with the primary objective to achieve continuous and efficient operations of IFTNs. In essence, logistics network design, as in [47,48], deals with strategic decisions defining network structure and capacity, while our work emphasizes tactical and operational maintenance decisions for uninterrupted function of already-constructed IFTNs.

(ii) Studies [47] and [49] investigate relationships and differences between robust models and other variants (e.g., stochastic models) to design new networks. In contrast, our work applies robust models and other variants to assess and maintain already-constructed IFTNs. Additionally, we conduct extensive numerical experiments to study the conservativeness of different models and their maintenance decisions for the already-constructed IFTN. Meanwhile, we evaluate key parameters to achieve managerial insights to operate already-constructed IFTNs. Consequently, the modeling and solution framework in this work can serve as a decision-support tool aiding in IFTN performance assessment and maintenance.

Based on the literature review, three distinct research gaps are identified as follows. Accordingly, these gaps are filled by this work as outlined in the last row of Table 1.

(i) The literature commonly focuses on vulnerability assessment for transportation networks, neglecting the crucial aspect of vulnerability reduction, which is essential to maintain uninterrupted function of already-constructed IFTNs.

(ii) Though some studies explore disruption uncertainties for single-modal transportation networks, there is a notable scarcity of research to address uncertain disruptions specific to already-constructed IFTNs for VA&R.

(iii) Existing research rarely addresses complete and partial failures in both nodes and links, especially intermodal links that connect different transportation modes, within the already-constructed IFTNs.

3. Problem Statement

This section elaborates on the problem of VA&R for already-constructed IFTNs considering the impact of uncertain disruptions in both nodes and links, including intermodal links that connect different transportation modes, as well as cascading failures and influence spreading.

3.1. Intermodal freight transportation network

The topology structure and properties of IFTN are presented, accompanied by notations for ease of problem formulation and necessary assumptions to make the modeling manageable.

3.1.1. Components and features

In the IFTN, a route comprises a sequence of links and their connected nodes, starting from an origin location and ending at a destination location. Typically, the route from an origin to a destination is segmented into three phases: pre-haul (e.g., the first-mile related to pickup process), long-haul (e.g., city-to-city transportation), and end-haul (e.g., the last-mile related to delivery process). Generally, pre-haul and end-haul are facilitated through road transportation. The long-haul segment, however, is diverse and can encompass multiple transportation modes, including road, railway, river, or sea. Notice that air transportation is seldom used to transport large containerized goods, such as twenty-foot equivalent unit (TEU) containers. Consequently, an IFTN can be viewed as a multi-layered network made up of several subnetworks. Each of these subnetworks aligns with a specific mode of transportation. For instance, Figure 2 presents an IFTN connecting China, the Middle East, and Europe. In this depiction: yellow represents the main roads in China, green denotes the main freight railways in China, purple indicates the Yangtze River, as well as blue and red symbolize the westbound and eastbound sea routes, respectively. Specifically, the sea subnetwork refers to the service route of a leading container shipping company.

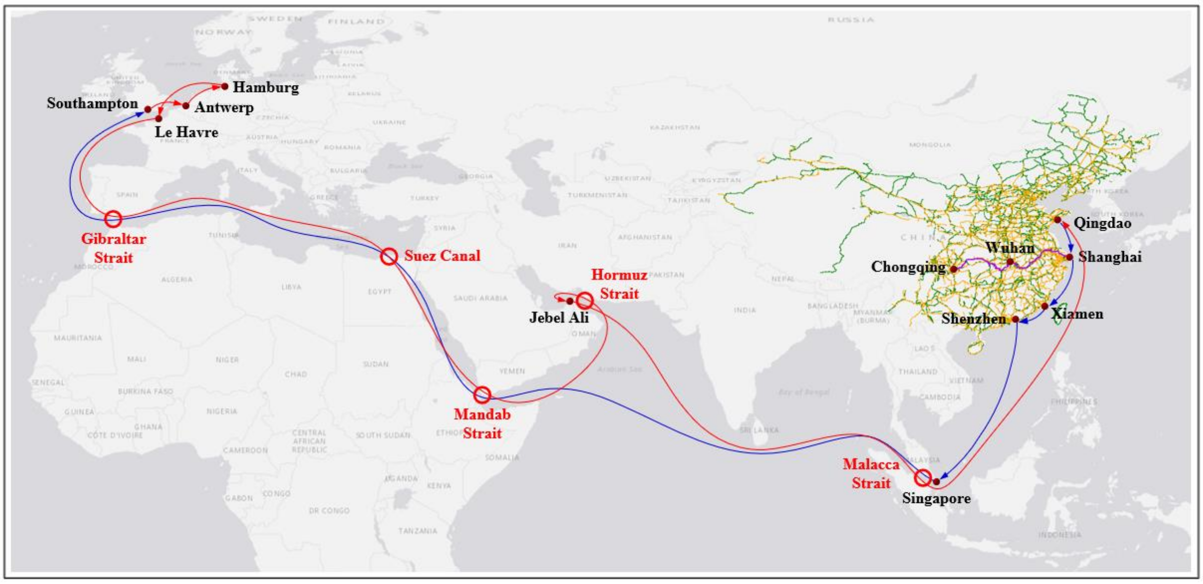

Figure 2. The IFTN connecting China, the Middle East, and Europe.

The IFTN includes four types of nodes. (i) *Origin* or *destination (OD) node*. Each origin node or destination node represents the freight supply or freight demand of the corresponding region, respectively. One node may simultaneously act as an origin node and a destination node. For example, node A in Figure 3 is an OD node. (ii) *Single-modal node*. One single-modal node connects links belonging to the same transportation mode (e.g., one railway station connecting multiple railway links). Thus, freight will not be changed to another mode at a single-modal node. In practice, a single-modal node may be a station on road/railway, or a port by river/sea. For example, nodes B, C, D, and G in Figure 3 are single-modal nodes. (iii) *Intermodal node*. One intermodal node connects links belonging to two or more transportation modes. Thus, freight can be switched between modes at an intermodal node. Intermodal nodes characterize the *interconnection* among different transportation modes, reflecting one fundamental difference between IFTNs and the single-modal transportation network. For example, nodes F, H, J, and K in Figure 3 are intermodal nodes. Specifically, the dashed circle including nodes F, G, and H in Figure 3 could represent a local area (e.g., a city), where multiple nodes exist closely. (iv) *Crossing node*. A crossing node is associated with multiple links, some of which are over other links without connecting them. For example, a bridge serves as a crossing node, where the road/railway on the bridge is over but does not connect the road/railway/river under the bridge. Crossing nodes characterize the *interdependence* between links that are not directly connected. Specifically, if one crossing node is disrupted, the capacity of all associated links will degrade. For instance, if a bridge collapses, the links on and under the bridge will be simultaneously disrupted. In Figure 3, nodes E and I are crossing nodes. For clarity, single-modal nodes, intermodal nodes, and crossing nodes are collectively referred to as *transit nodes*.

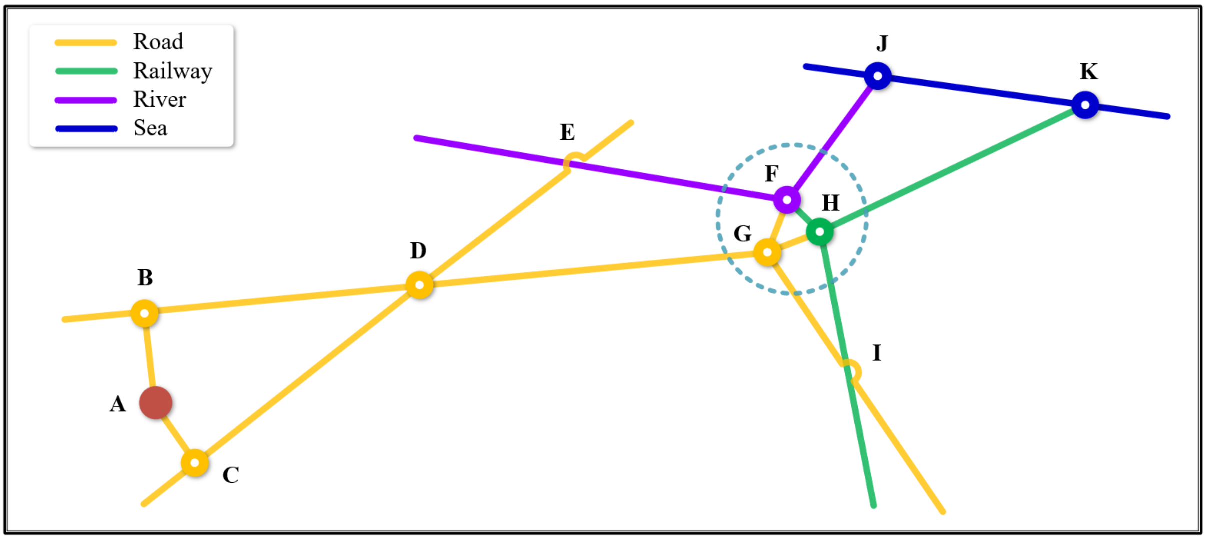

Figure 3. Depiction of nodes and links in an IFTN.

The IFTN contains three types of links. These links can be concisely explained based on the description of node types as aforementioned. (i) *OD link*, which connects one OD node and one transit node, typically represents the initial or final segment of a journey (e.g., links AB and AC in Figure 3). (ii) *Intermodal link*, which is the path to transfer freight between two transit nodes, each affiliated with a different transportation mode, within a local area (e.g., links FG, FH, and GH in Figure 3). (iii) *Transit link*, which connects two transit nodes and usually serves as city-to-city transportation (e.g., links BD, CD, DG, FJ, HK, and JK in Figure 3). The explicit consideration of intermodal links offers several benefits. It allows for a more detailed and granular analysis of the network, preserving the unique characteristics of individual transportation segments. This level of granularity is crucial for accurately assessing and reducing vulnerability of each segment, especially in scenarios where intermodal links play a key role. For instance, during the COVID-19 pandemic, urban disruptions had a significant impact on intermodal links, highlighting their importance in the overall network structure. Thus, the explicit integration of intermodal links not only accurately reflects the real structure of IFTNs, but also facilitates to examine the importance of these links, leading to a comprehensive identification of potential vulnerabilities and enhancing the network's reliability.

Accordingly, the IFTN exhibits a uniquely integrated and complex structure, different from single-modal and traditional multimodal transportation systems [50,51]. The distinct features of IFTNs are as follows, primarily stemming from integration of transportation modes and utilization of standardized containers, underscoring the need for specialized VA&R approaches.

(i) Integration of diverse transportation modes with standardized containers: IFTNs distinguish themselves from single-modal systems, which are limited to a single mode of transportation, by integrating an array of modes such as road, railway, river, and sea. This integration is further enhanced by the utilization of standardized containers, a feature that differentiates IFTNs from conventional multimodal systems. The adoption of standardized containers significantly enhances efficiency and seamlessness across diverse modes, markedly expediting the cascading failures and influence spreading in terms of timeliness and scope within the network.

(ii) Specialized intermodal nodes, and efficient and high-volume freight transportation: IFTNs are characterized by specialized intermodal nodes, which serve as pivotal points for cargo transfer across different transportation modes. These nodes are adept at performing efficient and high-volume container switching, an operational efficiency not typically found in single-modal or conventional multimodal systems. This efficiency and high-volume strengthen the interconnection and interdependency among nodes and links in IFTNs. Such a strengthened structure means that disruptions in the network can quickly trigger cascading effects across diverse modes, highlighting the need for specialized VA&R approaches.

3.1.2. Notations

An IFTN can be represented by a graph $\mathcal{G}=(\mathcal{N},\mathcal{L})$, consisting of nodes $\mathcal{N}$ and links $\mathcal{L}$. The IFTN involves all the common transportation modes, including road, railway, river, and sea. The network topology of each transportation mode serves as a subnetwork within the IFTN. Accordingly, the IFTN functions as a supergraph, integrating subnetworks for each transportation mode. The IFTN's performance is influenced by the routes from origins to destinations, and can be interpreted through the capacity conditions of nodes and links. Specifically, node $i\in\mathcal{N}$ possesses a capacity q_{node}^{i}, which imposes constraints on the freight flow passing through the node. Meanwhile, link $l \in \mathcal{L}$ has a capacity q_{link}^{l}, limiting the freight flow traversing the link. To specify the source of freight, term "*o*-freight" is used to represent the freight supplied from origin node $o \in \mathcal{N}_{\text{O}}$. Table 2 provides the list of notations for sets, parameters, and decision variables.

Table 2. List of notations.

Notation	Description
(i) Sets	
$\mathcal{G}$	The IFTN network, including nodes $\mathcal{N}$ and links $\mathcal{L}$, namely, $\mathcal{G} = (\mathcal{N}, \mathcal{L})$
$\mathcal{N}$	Set of nodes, specifically, $\mathcal{N} = \mathcal{N}_{\text{O}} \cup \mathcal{N}_{\text{D}} \cup \mathcal{N}_{\text{T}}$, where $\mathcal{N}_{\text{O}}$, $\mathcal{N}_{\text{D}}$ and $\mathcal{N}_{\text{T}}$ represent sets of origin nodes, destination nodes, and transit nodes, respectively
$\mathcal{L}$	Set of links, specifically, (i, j) and l can be interchangeably used to represent one link
$\mathcal{N}_i^-$	Set of predecessor nodes for node i, namely, $\mathcal{N}_i^- = \{ j \in \mathcal{N} \mid (j, i) \in \mathcal{L} \}$
$\mathcal{N}_i^+$	Set of successor nodes for node i, namely, $\mathcal{N}_i^+ = \{ j \in \mathcal{N} \mid (i, j) \in \mathcal{L} \}$
$\mathcal{D}$	Set of disruptive scenarios, specifically, $\mathcal{D}_k$ represents the kth set of disruptive scenarios if disruptive scenarios are categorized into K different sets, $\mathcal{D} = \bigcup_{k=1}^{K} \mathcal{D}_k$
$S(\cdot)$	Set of recourse actions, specifically, $S_k(\cdot)$ is the set of recourse actions for disruptive scenario set $\mathcal{D}_k$
(ii) Parameters	
q_{node}^{i}	Capacity of node $i \in \mathcal{N}$
q_{link}^{l}	Capacity of link $l \in \mathcal{L}$
m_i	Cost to implement full maintenance for element $i \in \mathcal{N} \cup \mathcal{L}$, specifically, m_{node}^{i} is the cost to implement full maintenance for node $i \in \mathcal{N}$, and m_{link}^{l} is the cost to implement full maintenance for link $l \in \mathcal{L}$
$c_{(i,j)}$	Transit cost of unit volume (e.g., one TEU) on link $(i, j) \in \mathcal{L}$; without loss of generality, the appliable operation cost at node i ($i \notin \mathcal{N}_{\text{D}}$) is included in the transit cost on link (i, j), and the appliable operation cost at node j ($j \in \mathcal{N}_{\text{D}}$) is included in the transit cost on link (i, j)
D	Demand matrix, specifically, $D_{(i,j)}$ is the freight demand from origin node $i \in \mathcal{N}_{\text{O}}$ to destination node $j \in \mathcal{N}_{\text{D}}$
v_o	Volume of *o*-freight, $o \in \mathcal{N}_{\text{O}}$
v_j^o	Volume of *o*-freight that is demanded at node $j \in \mathcal{N}_{\text{D}}$
θ_j^o	Penalty of unit volume of *o*-freight ($o \in \mathcal{N}_{\text{O}}$) that is demanded but unmet at node $j \in \mathcal{N}_{\text{D}}$

z_i	Equals 1 if element $i \in \mathcal{N} \cup \mathcal{L}$ is disrupted, and 0 otherwise
f_{node}	Limit on the number of simultaneously disrupted nodes, specifically, f_{node}^{k} is the limit on the number of simultaneously disrupted nodes in disruptive scenario set $\mathcal{D}_k$
f_{link}	Limit on the number of simultaneously disrupted links, specifically, f_{link}^{k} is the limit on the number of simultaneously disrupted links in disruptive scenario set $\mathcal{D}_k$
ρ_k	Weight of the *k*th disruptive scenario set $\mathcal{D}_k$, specifically, $\sum_{k=1}^{K} \rho_k = 1$ if disruptive scenarios are categorized into K different sets
α_i	Degree of degradation in the capacity of element $i \in \mathcal{N} \cup \mathcal{L}$, specifically, $0 \le \alpha_i \le 1$
M	A large number
ε_i	An exponential parameter to describe the nonlinear relationship between maintenance cost and maintenance benefit for element $i \in \mathcal{N} \cup \mathcal{L}$
(iii) Decision variables	
y_i	Degree of maintenance for element $i \in \mathcal{N} \cup \mathcal{L}$, $0 \le y_i \le 1$, specifically, y_{node}^{i} is the degree of maintenance for node $i \in \mathcal{N}$, and y_{link}^{l} is the degree of maintenance for link $l \in \mathcal{L}$
e_{y_i}	Cost to implement maintenance degree y_i for element $i \in \mathcal{N} \cup \mathcal{L}$
$x_{(i,j)}^{o}$	Volume of *o*-freight $\left(o \in \mathcal{N}_{\text{O}}\right)$ from node i to node j
u_j^{o}	Volume of unmet demand for *o*-freight $\left(o \in \mathcal{N}_{\text{O}}\right)$ at node $j \in \mathcal{N}_{\text{D}}$

3.1.3. Assumptions

To make the problem modeling manageable, necessary assumptions are made as follows.

(i) *System optimization.* Given the intrinsic interconnection and interdependence in logistics networks, along with cascading failures and influence spreading, it is imperative to optimize the network comprehensively, aiming for system-wide optimal solutions that benefit the entire system [52,53]. Accordingly, this work seeks to manage the IFTN from a system-optimum perspective.

(ii) *Freight assignment.* Considering the commercial nature of freight transportation, it is essential to employ shortest-path routing for freight assignments, respecting the capacity constraints of network elements. Thanks to modern communication technologies, carriers can ascertain the availability of network elements. This allows carriers to potentially reschedule freight flows under disruptive scenarios, minimizing the sum of transit costs and unmet-demand penalty costs.

(iii) *Operational features of crossing nodes.* To characterize the interdependence feature of crossing nodes, each crossing node can be represented as a set of dummy single-modal nodes, which locate closely to the original crossing node [27]. For example, in Figure 3, crossing node E can be represented as two dummy single-modal nodes, one on the road and the other on the river. The dummy single-modal node has the throughput capacity as the link on which it is located. Moreover, it is assumed that the dummy single-modal nodes experience a proportionate degradation in capacity under a disruption, reflecting the disruption degree of the crossing node.

(iv) *Network maintenance*. Maintenance of IFTN elements is crucial to prevent element failure and mitigate disruption hazards [7,54]. For example, dredging is an effective maintenance measure to keep the navigable depth and width of channels, which would otherwise cause ship accidents and disrupt ship transportation [7][55,56]. For another instance, the Suez Canal authority implemented maintenance actions after the blockage event in March 2021 to avert future disruptions. To maximize the benefit of maintenance, this work permits partial maintenance (as opposed to full maintenance) for element $i \in \mathcal{N} \cup \mathcal{L}$, correspondingly, element i will remain partial capacity under a disruption. The maintenance cost for element i is a function of maintenance degree, and we propose formula (1) to calculate the partial-maintenance cost referencing [54]. It should be emphasized that maintenance costs depend on various local factors, such as geological conditions, and the maintenance-cost function is not the focus of this work. Nevertheless, the following formula could be adapted to accommodate customized information:

$$e_{y_i} = \begin{cases} 0 \ \left(y_i = 0\right) \\ 0.15 m_i + 0.85 m_i y_i^{\varepsilon_i} \left(0 < y_i \le 1\right) \end{cases} \tag{1}$$

where e_{y_i} is the cost to implement maintenance degree y_i for element i; m_i is the cost of full maintenance for element i; $0.15m_i$ is the maintenance setup cost (regardless of maintenance degree), which is incurred for setting up maintenance equipment and affairs; and ε_i describes the nonlinear relationship between maintenance cost and maintenance benefit, typically, $\varepsilon_i > 1$. Though formula (1) is a piecewise function, $\min e_{y_i}$ can be linearized in minimization optimization as $\min 0.15 m_i r_i + 0.85 m_i y_i^{\varepsilon_i}$, subject to $0 \le y_i \le 1$, $y_i \le r_i$, and $r_i \in \{0,1\}$, where r_i is an introduced 0-1 variable.

3.2. Uncertain disruptions, cascading failures, and influence spreading

A disruption is defined as the failure of a single network element (i.e., node or link), represented by a binary variable, z_i $\left(i \in \mathcal{N} \cup \mathcal{L}\right)$, which indicates whether element i is disrupted. The uncertainty-set budget is defined as the maximum number of disrupted nodes f_{node}, and the maximum number of disrupted links f_{link}. Accordingly, the budgeted uncertainty set can be represented as:

$$\mathcal{D} = \left\{ \left(\mathbf{z}_{\text{node}}, \mathbf{z}_{\text{link}} \right) \mid \mathbf{z}_{\text{node}} \in \{0,1\}^{|\mathcal{N}|}, \mathbf{z}_{\text{link}} \in \{0,1\}^{|\mathcal{L}|}, \sum_{n \in \mathcal{N}} z_n \le f_{\text{node}}, \sum_{l \in \mathcal{L}} z_l \le f_{\text{link}} \right\} \tag{2}$$

where $z_n = 1$ if node n is disrupted, and $z_n = 0$ otherwise; similarly, $z_l = 1$ if link l is disrupted, and $z_l = 0$ otherwise. Without loss of generality, we assume that disruptions occur only at non-OD nodes. To account for disruptions at OD nodes, we can introduce dummy nodes representing supply and demand for the original OD nodes and treat the original OD nodes as transit nodes.

Considering the intricate interconnections and interdependencies in IFTNs, the budgeted uncertainty set (2) can yield various disruptive scenarios by combining multi-disruptions in nodes (including single-modal nodes, intermodal nodes, and crossing nodes) and links (including OD links, intermodal links, and transit links). For instance, in Figure 2, a bridge over the Yangtze River serves as a crossing node in the IFTN. If this bridge is damaged (e.g., bridge piers are struck by a ship), road and rail transportation on the bridge, as well as river transportation under the bridge, will be suspended for safety concerns. Furthermore, with varying values of f_{node} and f_{link}, a wide array of disruptive scenarios can be examined. Additionally, multiple uncertainty sets and partial failures are considered to further diversify uncertain disruptive scenarios.

Cascading failures in IFTNs can be characterized with depicting the causal relationship among them. In such scenarios, the failure of one element induces a compensatory load on alternative elements, making them more important in operations. The key alternative elements, under the strain of high-capacity operations, become increasingly vulnerable to failure [57]. Accordingly, cascading failures are captured by employing the “max” operator on the budgeted uncertainty set (2), accounting for the failures of key alternative elements for the worst-case scenarios (refer to objective functions (3), (5), (9), and (11)). Notice that, though cascading failures do not occur simultaneously, the interruption at one element can rapidly increase the logistics volume at alternative elements, a phenomenon exacerbated by modern communication technologies and the efficiency of IFTNs. Meanwhile, the impacts of cascading failures unfold cumulatively over a time period. Thus, the impacts of cascading failures are considered within a defined period for a comprehensive analysis of their consequences. Furthermore, the influence spreading among interconnected elements proceeds as follows. First, assuming that element i fails completely, the routes $\mathcal{R}$ containing element i become infeasible. This is because a feasible route requires all its constituent elements are functional. The route infeasibility subsequently affects the operations of other elements in routes $\mathcal{R}$. Let $\mathcal{R}'$ represent the alternative routes for routes $\mathcal{R}$. Consequently, routes $\mathcal{R}'$ will undertake additional freight transportation, affecting the operations of all elements in routes $\mathcal{R}'$. Second, assuming that element i partially fails, there will be a degradation in capacity of routes $\mathcal{R}$ that incorporate element i, influencing the operations of other elements in routes $\mathcal{R}$. Moreover, alternative routes $\mathcal{R}'$ will compensate for the disruption, influencing all elements in these alternative routes $\mathcal{R}'$. Thus, the IFTN can characterize how the failure of one element affects the operations of other elements, and reflect cascading failures and influence spreading.

4. Optimization Models

This section builds optimization models for the proposed VA&R problem tailored to already-constructed IFTNs. First, we present the basic VA&R models, which consider a single uncertainty set and assume that each disruption leads to a complete failure of the network element. Subsequently, we extend the basic models to account for multiple uncertainty sets and partial failures, enabling a comprehensive characterization of disruptive scenarios and enhancing the models' capabilities.

4.1. Basic VA&R models

As explained above, the vulnerability of IFTNs can be assessed by the increase in the sum of transit costs and unmet-demand penalty costs under a disruptive scenario. We calculate this sum value under disruption-free situation for a given demand matrix, then we calculate the sum value under the worst disruptive scenario within a budgeted uncertainty set for the same demand matrix. The vulnerability rate is defined as the percentage change in the sum value. Specifically, the basic vulnerability assessment (BVA) model is formulated as follows:

[BVA Model]:

$$\max_{(\mathbf{z}_{\text{node}},\mathbf{z}_{\text{link}})\in\mathcal{D}} \min_{\mathbf{x},\mathbf{u}\in S(\mathbf{z}_{\text{node}},\mathbf{z}_{\text{link}})} \left(\sum_{(i,j)\in\mathcal{L}} \sum_{o\in\mathcal{N}_{\text{O}}} c_{(i,j)} x^{o}_{(i,j)} + \sum_{j\in\mathcal{N}_{\text{D}}} \sum_{o\in\mathcal{N}_{\text{O}}} \theta^{o}_{j} u^{o}_{j} \right) / v_{\text{DM}} - 1 \tag{3}$$

$$\text{s.t. } S(\mathbf{z}_{\text{node}},\mathbf{z}_{\text{link}}) = \left\{ \begin{array}{l} \sum_{j\in\mathcal{N}_o^+} x^{o}_{(o,j)} \le v_o \quad \forall o\in\mathcal{N}_{\text{O}} \quad (4\text{-}1) \\ \sum_{j\in\mathcal{N}_i^-} x^{o}_{(j,i)} = \sum_{j\in\mathcal{N}_i^+} x^{o}_{(i,j)} \quad \forall o\in\mathcal{N}_{\text{O}},\ i\in\mathcal{N}_{\text{T}} \quad (4\text{-}2) \\ \sum_{i\in\mathcal{N}_j^-} x^{o}_{(i,j)} + u^{o}_{j} = v^{o}_{j} \quad \forall o\in\mathcal{N}_{\text{O}},\ j\in\mathcal{N}_{\text{D}} \quad (4\text{-}3) \\ \sum_{j\in\mathcal{N}_i^+} \sum_{o\in\mathcal{N}_{\text{O}}} x^{o}_{(i,j)} \le (1-z_i) q^{i}_{\text{node}} \quad \forall i\in\mathcal{N}_{\text{T}} \quad (4\text{-}4) \\ \sum_{o\in\mathcal{N}_{\text{O}}} x^{o}_{(i,j)} \le \left(1-z_{(i,j)}\right) q^{(i,j)}_{\text{link}} \quad \forall (i,j)\in\mathcal{L} \quad (4\text{-}5) \\ x^{o}_{(i,j)} \ge 0 \quad \forall o\in\mathcal{N}_{\text{O}},\ (i,j)\in\mathcal{L} \quad (4\text{-}6) \\ u^{o}_{i} \ge 0 \quad \forall o\in\mathcal{N}_{\text{O}},\ i\in\mathcal{N}_{\text{D}} \quad (4\text{-}7) \end{array} \right\} \tag{4}$$

where v_{DM} is the objective value of the DM (see Appendix A); set $\mathcal{D}$ defines the disruptive scenarios; and vectors $\mathbf{z}_{\text{node}}$ and $\mathbf{z}_{\text{link}}$ represent the disruptive status of nodes and links, respectively; set $S(\mathbf{z}_{\text{node}},\mathbf{z}_{\text{link}})$ comprises recourse decisions (i.e., freight rescheduling) under disruptive scenarios $\mathbf{z}_{\text{node}}$ and $\mathbf{z}_{\text{link}}$. Objective function (3) aims to calculate the vulnerability rate by minimizing the sum of transit costs and unmet-demand penalty costs under the worst disruptive scenario. Constraints (4-1) - (4-3) represent the freight flow for origin nodes, transit nodes, and destination nodes, respectively. Constraints (4-4) and (4-5) limit the freight flow, considering element capacity and disruptions. Constraints (4-6) and (4-7) define the variable domains.

As aforementioned, vulnerability reduction can be achieved by identifying key facilities and performing appropriate-level maintenance. This approach can alleviate the negative effects of disruptions [7]. To address uncertain disruptive events in the maintenance decision-making process, a basic vulnerability reduction (BVR) model based on two-stage robust optimization is developed. In the first stage, maintenance decisions are made to mitigate the impact of potential disruptive scenarios. In the second stage, recourse actions are calculated to reschedule freight transportation based on surviving elements and their associated capacities once the disruptive scenario is revealed.

[BVR Model]:

$$\min_{\mathbf{y}_{\text{node}},\mathbf{y}_{\text{link}}} \sum_{i\in\mathcal{N}_{\text{T}}} e_{y^{i}_{\text{node}}} + \sum_{(i,j)\in\mathcal{L}} e_{y^{(i,j)}_{\text{link}}} + \max_{(\mathbf{z}_{\text{node}},\mathbf{z}_{\text{link}})\in\mathcal{D}} \ \min_{\mathbf{x},\mathbf{u}\in S(\mathbf{y}_{\text{node}},\mathbf{y}_{\text{link}},\mathbf{z}_{\text{node}},\mathbf{z}_{\text{link}})} \left(\sum_{(i,j)\in\mathcal{L}} \sum_{o\in\mathcal{N}_{\text{O}}} c_{(i,j)} x^{o}_{(i,j)} + \sum_{j\in\mathcal{N}_{\text{D}}} \sum_{o\in\mathcal{N}_{\text{O}}} \theta^{o}_{j} u^{o}_{j} \right) \tag{5}$$

s.t. (1),

$$S\left(\mathbf{y}_{\text{node}},\mathbf{y}_{\text{link}},\mathbf{z}_{\text{node}},\mathbf{z}_{\text{link}}\right) = \left\{ \begin{array}{l} \sum\limits_{j\in\mathcal{N}^{+}_{o}} x^{o}_{(o,j)} \le v_{o} \quad \forall o\in\mathcal{N}_{\text{O}} \quad (6\text{-}1) \\ \sum\limits_{j\in\mathcal{N}^{-}_{i}} x^{o}_{(j,i)} = \sum\limits_{j\in\mathcal{N}^{+}_{i}} x^{o}_{(i,j)} \quad \forall o\in\mathcal{N}_{\text{O}},\ i\in\mathcal{N}_{\text{T}} \quad (6\text{-}2) \\ \sum\limits_{i\in\mathcal{N}^{-}_{j}} x^{o}_{(i,j)} + u^{o}_{j} = v^{o}_{j} \quad \forall o\in\mathcal{N}_{\text{O}},\ j\in\mathcal{N}_{\text{D}} \quad (6\text{-}3) \\ \sum\limits_{j\in\mathcal{N}^{+}_{i}} \sum\limits_{o\in\mathcal{N}_{\text{O}}} x^{o}_{(i,j)} \le \left(1 - z_{i}\left(1 - y^{i}_{\text{node}}\right)\right) q^{i}_{\text{node}} \quad \forall i\in\mathcal{N}_{\text{T}} \quad (6\text{-}4) \\ \sum\limits_{o\in\mathcal{N}_{\text{O}}} x^{o}_{(i,j)} \le \left(1 - z_{(i,j)}\left(1 - y^{(i,j)}_{\text{link}}\right)\right) q^{(i,j)}_{\text{link}} \quad \forall (i,j)\in\mathcal{L} \quad (6\text{-}5) \\ x^{o}_{(i,j)} \ge 0 \quad \forall o\in\mathcal{N}_{\text{O}},\ (i,j)\in\mathcal{L} \quad (6\text{-}6) \\ u^{o}_{i} \ge 0 \quad \forall o\in\mathcal{N}_{\text{O}},\ i\in\mathcal{N}_{\text{D}} \quad (6\text{-}7) \end{array} \right\} \tag{6}$$

$$y^{i}_{\text{node}} \in [0,1] \quad \forall i\in\mathcal{N}_{\text{T}} \tag{7}$$

$$y^{(i,j)}_{\text{link}} \in [0,1] \quad \forall (i,j)\in\mathcal{L} \tag{8}$$

where set $\mathcal{D}$ defines disruptive scenarios; vectors $\mathbf{z}_{\text{node}}$ and $\mathbf{z}_{\text{link}}$ represent the disruptive status of nodes and links, respectively; set $S(\mathbf{y}_{\text{node}},\mathbf{y}_{\text{link}},\mathbf{z}_{\text{node}},\mathbf{z}_{\text{link}})$ comprises recourse decisions under maintenance decisions $\mathbf{y}_{\text{node}}$ and $\mathbf{y}_{\text{link}}$ as well as disruptive scenarios $\mathbf{z}_{\text{node}}$ and $\mathbf{z}_{\text{link}}$. The BVR model aims to minimize the sum of maintenance costs, transit costs, and unmet-demand penalty costs in the worst-case disruptive scenario within the budgeted uncertainty set. The model's constraints (6-1) - (6-3) limit the freight flow for origin, transit, and destination nodes, respectively. Constraints (6-4) and (6-5) limit freight flow based on element capacity, disruptions, and maintenance. Specifically, the degree of degradation in an element's capacity is inversely correlated with the degree of maintenance performed for the element. Constraints (6-6), (6-7), (7), and (8) define the domain of variables. In summary, the BVR model provides an approach to vulnerability reduction by incorporating uncertain disruptive events into maintenance decision-making.

4.2. Model extension and comparison

In this section, we enhance the basic VA&R models by incorporating multiple uncertainty sets and accounting for partial failures, drawing inspiration from the research on logistics and power network design [47–49]. These modifications are crucial for representing a diverse range of disruptive scenarios and offering increased practical utility. Furthermore, we compare the basic VA&R models with their extended counterparts, DM (see Appendix A), and SP-based VA&R models (see Appendix B).

(i) Integration of multiple uncertainty sets

The uncertainty set is a significant factor influencing the performance of IFTNs. However, a single uncertainty set with a small budget (i.e., f_{node} and f_{link}) is insufficient to capture diverse scenarios, while a single uncertainty set with a large budget can lead to over-conservative and costly solutions. Thus, it is more practical to adopt multiple uncertainty sets $\mathcal{D}_k\left(k=1,\ldots,K\right)$ to depict disruptive scenarios [49]. Each uncertainty set is associated with a weight ρ_k ($0<\rho_k\le 1$, $\sum_{k=1}^{K}\rho_k=1$), which represents the decision maker's confidence in the set and the willingness to undertake maintenance. The weight assigned to each uncertainty set impacts resource and maintenance costs, hence, changes in the weight of each set can alter the objective value. The models incorporating multiple uncertainty sets are referred to as multi-set VA&R models. Specifically, the multi-set vulnerability assessment (MVA) model is formulated as follows:

[MVA Model]:

$$\sum_{k=1}^{K}\rho_k\left(\max_{(\mathbf{z}_{\text{node}},\mathbf{z}_{\text{link}})\in\mathcal{D}_k}\ \min_{\mathbf{x},\mathbf{u}\in S_k(\mathbf{z}_{\text{node}},\mathbf{z}_{\text{link}})}\left(\sum_{(i,j)\in\mathcal{L}}\sum_{o\in\mathcal{N}_{\text{O}}}c_{(i,j)}x_{(i,j)}^{o}+\sum_{j\in\mathcal{N}_{\text{D}}}\sum_{o\in\mathcal{N}_{\text{O}}}\theta_j^o u_j^o\right)\right)/v_{\text{DM}}-1 \tag{9}$$

$$\text{s.t. } S_k\left(\mathbf{z}_{\text{node}},\mathbf{z}_{\text{link}}\right)=\left\{\begin{array}{l}
\sum_{j\in\mathcal{N}_o^+}x_{(o,j)}^{o}\le v_o\quad \forall o\in\mathcal{N}_{\text{O}}\quad (10\text{-}1)\\
\sum_{j\in\mathcal{N}_i^-}x_{(j,i)}^{o}=\sum_{j\in\mathcal{N}_i^+}x_{(i,j)}^{o}\quad \forall o\in\mathcal{N}_{\text{O}},\ i\in\mathcal{N}_{\text{T}}\quad (10\text{-}2)\\
\sum_{i\in\mathcal{N}_j^-}x_{(i,j)}^{o}+u_j^o=v_j^o\quad \forall o\in\mathcal{N}_{\text{O}},\ j\in\mathcal{N}_{\text{D}}\quad (10\text{-}3)\\
\sum_{j\in\mathcal{N}_i^+}\sum_{o\in\mathcal{N}_{\text{O}}}x_{(i,j)}^{o}\le\left(1-z_i\right)q_{\text{node}}^{i}\quad \forall i\in\mathcal{N}_{\text{T}}\quad (10\text{-}4)\\
\sum_{o\in\mathcal{N}_{\text{O}}}x_{(i,j)}^{o}\le\left(1-z_{(i,j)}\right)q_{\text{link}}^{(i,j)}\quad \forall (i,j)\in\mathcal{L}\quad (10\text{-}5)\\
x_{(i,j)}^{o}\ge 0\quad \forall o\in\mathcal{N}_{\text{O}},\ (i,j)\in\mathcal{L}\quad (10\text{-}6)\\
u_i^o\ge 0\quad \forall o\in\mathcal{N}_{\text{O}},\ i\in\mathcal{N}_{\text{D}}\quad (10\text{-}7)
\end{array}\right\} \tag{10}$$

Additionally, the multi-set vulnerability reduction (MVR) model is formulated with objective function (11), constraints (1), (7), and (8), in conjunction with constraint (12) pertaining to recourse set $S_k(\mathbf{y}_{\text{node}},\mathbf{y}_{\text{link}},\mathbf{z}_{\text{node}},\mathbf{z}_{\text{link}})$.

[MVR Model]:

$$\min_{\mathbf{y}_{\text{node}},\mathbf{y}_{\text{link}}} \sum_{i\in\mathcal{N}_{\text{T}}} e_{y^i_{\text{node}}} + \sum_{(i,j)\in\mathcal{L}} e_{y^{(i,j)}_{\text{link}}} + \sum_{k=1}^{K}\rho_k\left(\max_{\substack{(\mathbf{z}_{\text{node}},\mathbf{z}_{\text{link}})\\ \in\mathcal{D}_k}} \min_{\substack{\mathbf{x},\mathbf{u}\\ \in S_k(\mathbf{y}_{\text{node}},\mathbf{y}_{\text{link}},\mathbf{z}_{\text{node}},\mathbf{z}_{\text{link}})}} \left(\sum_{(i,j)\in\mathcal{L}}\sum_{o\in\mathcal{N}_{\text{O}}} c_{(i,j)}x^o_{(i,j)} + \sum_{j\in\mathcal{N}_{\text{D}}}\sum_{o\in\mathcal{N}_{\text{O}}}\theta^o_j u^o_j\right)\right) \quad (11)$$

s.t. (1), (7), and (8),

$$S_k(\mathbf{y}_{\text{node}},\mathbf{y}_{\text{link}},\mathbf{z}_{\text{node}},\mathbf{z}_{\text{link}}) = \left\{\begin{array}{ll} \sum_{j\in\mathcal{N}_o^+} x^o_{(o,j)} \le v_o \quad \forall o\in\mathcal{N}_{\text{O}} & (12\text{-}1)\\ \sum_{j\in\mathcal{N}_i^-} x^o_{(j,i)} = \sum_{j\in\mathcal{N}_i^+} x^o_{(i,j)} \quad \forall o\in\mathcal{N}_{\text{O}},\ i\in\mathcal{N}_{\text{T}} & (12\text{-}2)\\ \sum_{i\in\mathcal{N}_j^-} x^o_{(i,j)} + u^o_j = v^o_j \quad \forall o\in\mathcal{N}_{\text{O}},\ j\in\mathcal{N}_{\text{D}} & (12\text{-}3)\\ \sum_{j\in\mathcal{N}_i^+}\sum_{o\in\mathcal{N}_{\text{O}}} x^o_{(i,j)} \le \left(1-z_i\left(1-y^i_{\text{node}}\right)\right)q^i_{\text{node}} \quad \forall i\in\mathcal{N}_{\text{T}} & (12\text{-}4)\\ \sum_{o\in\mathcal{N}_{\text{O}}} x^o_{(i,j)} \le \left(1-z_{(i,j)}\left(1-y^{(i,j)}_{\text{link}}\right)\right)q^{(i,j)}_{\text{link}} \quad \forall (i,j)\in\mathcal{L} & (12\text{-}5)\\ x^o_{(i,j)} \ge 0 \quad \forall o\in\mathcal{N}_{\text{O}},\ (i,j)\in\mathcal{L} & (12\text{-}6)\\ u^o_i \ge 0 \quad \forall o\in\mathcal{N}_{\text{O}},\ i\in\mathcal{N}_{\text{D}} & (12\text{-}7) \end{array}\right\} \quad (12)$$

(ii) Consideration of partial failures

An additional enhancement to the VA&R model accommodates partial failures of elements. For instance, several Chinese ports experienced partial closures due to strict public health measures during the peak of COVID-19 pandemic. Thus, a parameter α_i $(0\le\alpha_i\le1)$ is introduced to represent the degree of capacity degradation for an element i. The partial-failure constraints (13) and (14) are applied to the BVA model, replacing constraints (4-4) and (4-5), to generate the partial-failure vulnerability assessment model. Similarly, the partial-failure constraints (15) and (16) are applied to the BVR model, replacing constraints (6-4) and (6-5), to generate the partial-failure vulnerability reduction model. These two models are collectively referred to as partial-failure VA&R models. Additionally, the partial-failure constraints (13) and (14) can be applied to the MVA model, replacing constraints (10-4) and (10-5), to establish the partial-failure MVA model. Likewise, the partial-failure constraints (15) and (16) can be applied to the MVR model, replacing constraints (12-4) and (12-5), to establish the partial-failure MVR model. These two models are collectively referred to as PMVA&R models.

$$\sum_{j \in \mathcal{N}_i^+} \sum_{o \in \mathcal{N}_\mathrm{O}} x_{(i,j)}^o \le \left(1 - \alpha_i z_i\right) q_\mathrm{node}^i \quad \forall i \in \mathcal{N}_\mathrm{T} \tag{13}$$

$$\sum_{o \in \mathcal{N}_\mathrm{O}} x_{(i,j)}^o \le \left(1 - \alpha_{(i,j)} z_{(i,j)}\right) q_\mathrm{link}^{(i,j)} \quad \forall (i,j) \in \mathcal{L} \tag{14}$$

$$\sum_{j \in \mathcal{N}_i^+} \sum_{o \in \mathcal{N}_\mathrm{O}} x_{(i,j)}^o \le \left(1 - \alpha_i z_i \left(1 - y_\mathrm{node}^i\right)\right) q_\mathrm{node}^i \quad \forall i \in \mathcal{N}_\mathrm{T} \tag{15}$$

$$\sum_{o \in \mathcal{N}_\mathrm{O}} x_{(i,j)}^o \le \left(1 - \alpha_{(i,j)} z_{(i,j)} \left(1 - y_\mathrm{link}^{(i,j)}\right)\right) q_\mathrm{link}^{(i,j)} \quad \forall (i,j) \in \mathcal{L} \tag{16}$$

(iii) Comparisons and discussions

Basic VA&R models employ a single uncertainty set to represent disruptive scenarios. In contrast, multi-set VA&R models and partial-failure VA&R models incorporate multiple uncertainty sets and partial failures, respectively. PMVA&R models consider both multiple uncertainty sets and partial failures simultaneously. As such, basic VA&R models constitute a specific instance of multi-set VA&R models with $K = 1$ (i.e., one uncertainty set), a particular instance of partial-failure VA&R models with $\alpha_i = 1$ (i.e., no partial failure), and a special case of PMVA&R models with $K = 1$ and $\alpha_i = 1$ (i.e., one uncertainty set and no partial failure). Both basic VA&R models and partial-failure VA&R models aim to minimize the worst-case cost, while multi-set VA&R models and PMVA&R models identify the worst disruptive scenario in each uncertainty set $\mathcal{D}_k$ $\left(k = 1,...,K\right)$ and calculate the weighted sum of worst-case costs.

Furthermore, we compare the basic and extended VA&R models (including basic VA&R, multi-set VA&R, partial-failure VA&R, and PMVA&R models) with DM and SP-based VA&R models. Based on our evaluation, we derive the following conclusions: *(a)* DM represents a special case of basic VA&R models with $f_\mathrm{node} = 0$ and $f_\mathrm{link} = 0$ (i.e., no disruption events), and a special case of multi-set VA&R models and PMVA&R models with $K = 0$ (i.e., no disruptive scenarios). *(b)* SP-based VA&R models without partial failure are equivalent to multi-set VA&R models, where each uncertainty set includes only one disruptive scenario; similarly, SP-based VA&R models with partial failure are equivalent to PMVA&R models, where each uncertainty set contains only one disruptive scenario. Figure 4 illustrates the relationships and transformations among basic and extended VA&R models, DM, and SP-based VA&R models.

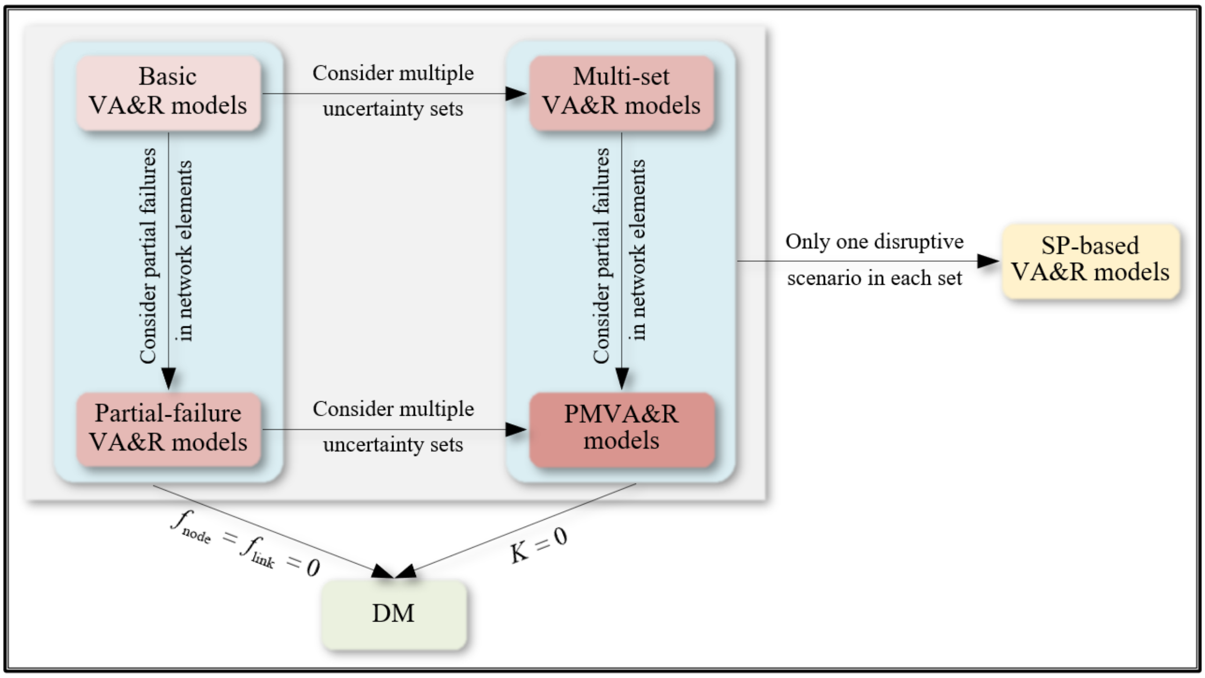

Figure 4. Relationships and transformations among the models.

5. Solution Method

The VA&R models involve two-stage robust optimization, which presents significant challenges to find optimal solutions [41]. Fortunately, the C&CG algorithm framework has proven effective in addressing challenges for relevant problems, such as designing yet-to-be-constructed transportation networks [45–48]. Thus, this work explores the C&CG algorithm framework along with speedup strategies by considering problem features and model structures of VA&R, specifically tailored for already-constructed IFTNs.

5.1. The C&CG algorithm

The C&CG algorithm operates through a master-subproblem interaction framework, where the solution to the master problem (MP) serves as input to the subproblem. As the subproblem is a max-min problem, we use duality to transform it into a max-max problem, which is subsequently integrated into a maximization problem. As penalties arise from unmet demand, the subproblem consistently maintains feasibility. In this subsection, we elucidate the details of the C&CG algorithm for the BVR model. Other models can be solved by analogy with minor adjustments. For example, when solving the BVA model, the technique to transform the max-min subproblem into a maximization problem using duality remains identical to that of the BVR model.

5.1.1. Dual of the second-stage problem

Dual variables $\boldsymbol{\lambda}$, $\boldsymbol{\mu}$, $\boldsymbol{\gamma}$, $\boldsymbol{\pi}$, and $\boldsymbol{\xi}$ are introduced for constraints (6-1) - (6-5), respectively. The dual subproblem is formulated as follows:

[NonL-SubP]:

$$\max \sum_{o\in\mathcal{N}_{\mathrm{O}}} v_o\lambda_o - \sum_{i\in\mathcal{N}_{\mathrm{D}}}\sum_{o\in\mathcal{N}_{\mathrm{O}}} v_i^o\gamma_i^o + \sum_{i\in\mathcal{N}_{\mathrm{T}}}\left(1-z_i\left(1-\hat{y}_{\mathrm{node}}^i\right)\right)q_{\mathrm{node}}^i\pi_i + \sum_{(i,j)\in\mathcal{L}}\left(1-z_{(i,j)}\left(1-\hat{y}_{\mathrm{link}}^{(i,j)}\right)\right)q_{\mathrm{link}}^{(i,j)}\xi_{(i,j)} \tag{17}$$

$$\text{s.t. } \lambda_o + \mu_j^o \le c_{(o,j)} \quad \forall o\in\mathcal{N}_{\mathrm{O}}, j\in\mathcal{N}_o^+ \tag{18}$$

$$-\mu_i^o + \mu_j^o + \pi_i + \xi_{(i,j)} \le c_{(i,j)} \quad \forall o\in\mathcal{N}_{\mathrm{O}},\ i\in\mathcal{N}_{\mathrm{T}}, j\in\mathcal{N}_i^+\cap\mathcal{N}_{\mathrm{T}} \tag{19}$$

$$-\mu_i^o + \gamma_i^o + \pi_i \le c_{(i,j)} \quad \forall o\in\mathcal{N}_{\mathrm{O}},\ i\in\mathcal{N}_{\mathrm{T}}, j\in\mathcal{N}_i^+\cap\mathcal{N}_{\mathrm{D}} \tag{20}$$

$$\gamma_j^o \le \theta_j^o \quad \forall o\in\mathcal{N}_{\mathrm{O}}, j\in\mathcal{N}_{\mathrm{D}} \tag{21}$$

$$\xi_{(i,j)} \le 0 \quad \forall (i,j)\in\mathcal{L} \tag{22}$$

$$\lambda_o \le 0 \quad \forall o\in\mathcal{N}_{\mathrm{O}} \tag{23}$$

$$\pi_i \le 0 \quad \forall i\in\mathcal{N}_{\mathrm{T}} \tag{24}$$

$$\mu_i^o \text{ free} \tag{25}$$

$$\left(\mathbf{z}_{\mathrm{node}},\mathbf{z}_{\mathrm{link}}\right)\in\mathcal{D} \tag{26}$$

The dual model (17) - (26) searches for the disruptive scenario (i.e., values of z_i and $z_{(i,j)}$) that maximizes the sum of transit costs and unmet-demand penalty costs. Notice that multiplication $z_i\pi_i$ and multiplication $z_{(i,j)}\xi_{(i,j)}$ render the model nonlinear. To linearize the model, we substitute $z_i\pi_i$ with variable w_i and introduce constraints (27) - (30) for variable w_i. Likewise, we replace $z_{(i,j)}\xi_{(i,j)}$ with variable $w'_{(i,j)}$ and introduce constraints (31) - (34) for variable $w'_{(i,j)}$.

$$w_i \le \pi_i + M_i\left(1-z_i\right) \quad \forall i\in\mathcal{N}_{\mathrm{T}} \tag{27}$$

$$w_i \le 0 \quad \forall i\in\mathcal{N}_{\mathrm{T}} \tag{28}$$

$$w_i \ge \pi_i \quad \forall i\in\mathcal{N}_{\mathrm{T}} \tag{29}$$

$$w_i \ge -M_i z_i \quad \forall i\in\mathcal{N}_{\mathrm{T}} \tag{30}$$

$$w'_{(i,j)} \le \xi_{(i,j)} + M_{(i,j)}\left(1 - z_{(i,j)}\right) \quad \forall (i,j) \in \mathcal{L} \tag{31}$$

$$w'_{(i,j)} \le 0 \quad \forall (i,j) \in \mathcal{L} \tag{32}$$

$$w'_{(i,j)} \ge \xi_{(i,j)} \quad \forall (i,j) \in \mathcal{L} \tag{33}$$

$$w'_{(i,j)} \ge -M_{(i,j)} z_{(i,j)} \quad \forall (i,j) \in \mathcal{L} \tag{34}$$

As a result, the linearized subproblem is presented as follows:

[L-SubP]:

$$\chi = \max \sum_{i\in\mathcal{N}_{\mathrm{O}}} v_o\lambda_o - \sum_{i\in\mathcal{N}_{\mathrm{D}}}\sum_{o\in\mathcal{N}_{\mathrm{O}}} v_i^o\gamma_i^o + \sum_{i\in\mathcal{N}_{\mathrm{T}}} q^i_{\mathrm{node}}\left(\pi_i - w_i + w_i\hat{y}^i_{\mathrm{node}}\right) + \sum_{(i,j)\in\mathcal{L}} q^{(i,j)}_{\mathrm{link}}\left(\xi_{(i,j)} - w'_{(i,j)} + w'_{(i,j)}\hat{y}^{(i,j)}_{\mathrm{link}}\right) \tag{35}$$

subject to constraints (18) - (34). Therefore, the BVR model can be effectively solved as a linear programming problem.

5.1.2. Algorithmic procedure

The C&CG algorithm and corresponding MP are presented as follows. During each iteration r, we calculate the worst disruptive scenario $\mathbf{z}^r$ by solving the linearized subproblem L-SubP. Subsequently, we create recourse variables $\left(\mathbf{x}^r, \mathbf{u}^r\right)$ and associated constraints, which are then incorporated into the MP. Let $Gap = \left(UB - LB\right)/LB$, where LB and UB denote the lower bound and upper bound, respectively. Let δ represent the optimality tolerance. The C&CG algorithm for solving the BVR model is implemented through the following steps:

Step 0: Initialize $LB = -\infty$, $UB = +\infty$, and $r = 0$.

Step 1: Solve the MP (36) - (46) to obtain a solution $\left(\mathbf{y}_{\mathrm{node}},\ \mathbf{y}_{\mathrm{link}},\ \phi\right)$. Assign the optimal value of the MP (36) - (46) to the *LB*.

Step 2: Solve the linearized subproblem L-SubP with respect to $\mathbf{y}_{\mathrm{node}}$ and $\mathbf{y}_{\mathrm{link}}$ to identify the worst disruptive scenario $\mathbf{z}^r$, and its corresponding optimal value χ^r. Assign value $\min\left\{UB, \sum_{i\in\mathcal{N}_{\mathrm{T}}} e_{y^i_{\mathrm{node}}} + \sum_{(i,j)\in\mathcal{L}} e_{y^{(i,j)}_{\mathrm{link}}} + \chi^r\right\}$ to the *UB*.

Step 3: If $Gap \le \delta$, terminate and output the solution. Otherwise, generate recourse variables $\left(\mathbf{x}^r, \mathbf{u}^r\right)$

and constraints related to disruptive scenario $\mathbf{z}^r$, and incorporate them into the MP (36) - (46). Update $r = r+1$ and return to *Step 1*.

[MP]:

$$\min \sum_{i\in\mathcal{N}_{\mathrm{T}}} e_{y^i_{\mathrm{node}}} + \sum_{(i,j)\in\mathcal{L}} e_{y^{(i,j)}_{\mathrm{link}}} + \phi \tag{36}$$

$$\text{s.t. } \phi \ge \sum_{(i,j)\in\mathcal{L}} \sum_{o\in\mathcal{N}_{\mathrm{O}}} c_{(i,j)} x^{o,e}_{(i,j)} + \sum_{j\in\mathcal{N}_{\mathrm{D}}} \sum_{o\in\mathcal{N}_{\mathrm{O}}} \theta^o_j u^{o,e}_j \quad \forall e\in\{1,2,...,r\} \tag{37}$$

$$\sum_{j\in\mathcal{N}^+_o} x^{o,e}_{(o,j)} \le v_o \quad \forall o\in\mathcal{N}_{\mathrm{O}},\ e\in\{1,2,...,r\} \tag{38}$$

$$\sum_{j\in\mathcal{N}^-_i} x^{o,e}_{(j,i)} = \sum_{j\in\mathcal{N}^+_i} x^{o,e}_{(i,j)} \quad \forall o\in\mathcal{N}_{\mathrm{O}},\ i\in\mathcal{N}_{\mathrm{T}},\ e\in\{1,2,...,r\} \tag{39}$$

$$\sum_{i\in\mathcal{N}^-_j} x^{o,e}_{(i,j)} + u^{o,e}_j = v^o_j \quad \forall o\in\mathcal{N}_{\mathrm{O}},\ j\in\mathcal{N}_{\mathrm{D}},\ e\in\{1,2,...,r\} \tag{40}$$

$$\sum_{j\in\mathcal{N}^+_i} \sum_{o\in\mathcal{N}_{\mathrm{O}}} x^{o,e}_{(i,j)} \le \left(1 - z^e_i\left(1 - y^i_{\mathrm{node}}\right)\right) q^i_{\mathrm{node}} \quad \forall i\in\mathcal{N}_{\mathrm{T}},\ e\in\{1,2,...,r\} \tag{41}$$

$$\sum_{o\in\mathcal{N}_{\mathrm{O}}} x^{o,e}_{(i,j)} \le \left(1 - z^e_{(i,j)}\left(1 - y^{(i,j)}_{\mathrm{link}}\right)\right) q^{(i,j)}_{\mathrm{link}} \quad \forall (i,j)\in\mathcal{L},\ e\in\{1,2,...,r\} \tag{42}$$

$$x^{o,e}_{(i,j)} \ge 0 \quad \forall o\in\mathcal{N}_{\mathrm{O}},\ (i,j)\in\mathcal{L},\ e\in\{1,2,...,r\} \tag{43}$$

$$u^{o,e}_i \ge 0 \quad \forall o\in\mathcal{N}_{\mathrm{O}},\ i\in\mathcal{N}_{\mathrm{D}},\ e\in\{1,2,...,r\} \tag{44}$$

$$y^i_{\mathrm{node}} \in [0,1] \quad \forall i\in\mathcal{N}_{\mathrm{T}} \tag{45}$$

$$y^{(i,j)}_{\mathrm{link}} \in [0,1] \quad \forall (i,j)\in\mathcal{L} \tag{46}$$

Moreover, to implement the benchmark algorithm BD, a cutting plane

$$\phi \ge \sum_{o\in\mathcal{N}_{\mathrm{O}}} v_o \lambda^r_o - \sum_{i\in\mathcal{N}_{\mathrm{D}}} \sum_{o\in\mathcal{N}_{\mathrm{O}}} v^o_i \gamma^{o,r}_i + \sum_{i\in\mathcal{N}_{\mathrm{T}}} \left(1 - z^r_i\left(1 - \hat{y}^i_{\mathrm{node}}\right)\right) q^i_{\mathrm{node}} \pi^r_i + \sum_{(i,j)\in\mathcal{L}} \left(1 - z^r_{(i,j)}\left(1 - \hat{y}^{(i,j)}_{\mathrm{link}}\right)\right) q^{(i,j)}_{\mathrm{link}} \xi^r_{(i,j)} \tag{47}$$

is iteratively added to the MP.

Remarks: For the MVR model, the objective function of the MP is modified to (48):

$$\min \sum_{i\in\mathcal{N}_{\mathrm{T}}} e_{y^i_{\mathrm{node}}} + \sum_{(i,j)\in\mathcal{L}} e_{y^{(i,j)}_{\mathrm{link}}} + \sum_{k=1}^{K} \rho_k \phi_k \tag{48}$$

where ϕ_k corresponds to uncertainty set $\mathcal{D}_k\ (k = 1,...,K)$. For each uncertainty set, a subproblem is solved to determine the worst disruptive scenario. Recourse variables and corresponding constraints are then generated and incorporated into the MP.

5.2. Algorithm improvement

To expedite the solution process of VA&R for the IFTN, we employ two strategies referencing the speedup techniques utilized in the facility location problem [46]. These strategies facilitate rapid identification of valid lower bounds, subsequently reducing the feasible solution space of the MP and enhancing computational efficiency. The C&CG algorithm incorporating the following two *varying* strategies is denoted as the "C&CG Vary" algorithm.

(i) *Varying disruptive scenarios.* In each iteration, the C&CG algorithm generates a single disruptive scenario, and each disruptive scenario corresponds to a lower bound. By exploring more significant disruptive scenarios in each iteration, a superior lower bound can be obtained. Specifically, during iteration r, given a disruptive scenario $\mathbf{z}^r$ by solving the subproblem L-SubP, an additional disruptive scenario can be produced by changing the disrupted elements with the least freight flow to non-disrupted and changing the non-disrupted elements with the largest freight flow to disrupted. Simultaneously, duplicate disruptive scenarios are eliminated. This variation of disruptive scenarios expedites the enhancement of the lower bound. Notice that this speedup strategy requires extra time for probing variables and results in the MP with a higher number of disruptive scenarios, making it especially effective for larger instances.

(ii) *Varying optimality tolerance.* In the initial iterations, the gap between lower and upper bounds is generally large. Pursuing the optimal solution for the MP is unnecessary, as a satisfactory feasible solution suffices to generate a significantly disruptive scenario. Consequently, a relatively large optimality tolerance for MP solutions can be set during the early stage. As the gap narrows, smaller optimality tolerances are required to achieve more precise lower bounds. This speedup strategy is particularly effective for large instances, wherein the MP represents a large-scale mixed-integer programming problem and is computationally demanding.

6. Numerical Experiments

The numerical experiments have two main goals regarding already-constructed IFTNs. First, effectiveness and efficiency of the VA&R models and the C&CG algorithm with speedup strategies are demonstrated. To validate this, the basic and extended VA&R models are compared with the DM and SP-based VA&R models; meanwhile, a comparative analysis between the C&CG algorithm and the benchmark BD algorithm is undertaken to emphasize the superior performance of the C&CG algorithm. Second, the numerical experiments aim to derive managerial insights into VA&R, providing valuable references for practical operations. To this end, sensitivity analysis is performed to evaluate the impact of disruptions and maintenance (see Section 6.4.1), weights of uncertainty sets (see Section 6.4.2), and partial failure alongside uncertainty-set budgets (see Section 6.4.3). To ensure unbiased insights, numerical experiments are conducted on a real-world IFTN, and the results are averaged over 20 instances for each particular setting.

The modeling and solution methods are coded using Python 3.7, with Gurobi 9.0.1 employed as a general-purpose solver. The numerical experiments are conducted on Intel(R) Xeon(R) CPU E5-2680 with 2.40 GHz and 32 GB RAM under Linux 4.4.0.

6.1. Problem instances

The problem instances are generated based on the real-world IFTN shown in Figure 2. This network prominently features roads and railways, forming the crux of land freight transportation within China - a pivotal region in global freight movement. Furthermore, the sea subnetwork is meticulously designed to establish a corridor that connects China and Europe, with bridging the Middle East. The sea subnetwork's design is informed by the operational routes of a leading container shipping company. In our pursuit of rendering the IFTN more representative, we integrate the river transportation mode, specifically, the Yangtze River. This deliberate inclusion serves to encompass all four predominant transportation modes within IFTNs: road, railway, river, and sea.

The instance generation is divided into three aspects:

(i) *Network topology*. The road, railway, and river subnetworks are created using the database provided by the National Geomatics Center of China. The road subnetwork includes freeways and high-grade roads, while the railway subnetwork consists of freight-capable lines. The sea subnetwork is created using three-month global AIS data of container ships and referencing the service of a leading container shipping company. Crossing nodes are manually placed using civil engineering information. The entire IFTN consists of 85 transit nodes (including 35 stations on roads, 20 stations on railways, 10 ports on the Yangtze River, 10 sea ports, and 10 crossing nodes), 650 transit and intermodal links, and up to 50 OD nodes. Although road, railway, and river modes are only considered within China for the case study, our modeling and solution methods can be applied to other regions where road, railway, and river transportations are involved. To gain a detailed understanding of the sea subnetwork, our study employs a comparative analysis. Specifically, it contrasts sea elements within China (where diverse alternative transportation options are available) with those situated outside China (where such alternatives are limited or absent). This comparative approach is vital for an in-depth assessment of vulnerability and strategic significance of different sea segments. Furthermore, it provides insights into how the geographical positioning of sea elements impacts their importance.

(ii) *Node attributes, link attributes, and freight demand*. Node $i \in \mathcal{N}_\mathrm{T}$ has two attributes: capacity q^i_node and full-maintenance cost m^i_node. Capacity q^i_node is set to the real-world throughput capacity value, and full-maintenance cost m^i_node is related to the transportation mode and positively correlated with node capacity. Link $l \in \mathcal{L}$ has three attributes: capacity q^l_link, transit cost per TEU c_l, and full-maintenance cost m^l_link. The first two parameters are set based on real-world statistical data, while full-maintenance cost m^l_link is related to transportation mode and positively correlated with the link capacity and length. Freight supply and demand are measured by the number of TEU containers. The supply volume from node $o \in \mathcal{N}_\mathrm{O}$ and the demand volume at node $j \in \mathcal{N}_\mathrm{D}$ are derived from historical container throughput data. Additionally, a penalty cost θ^o_j is set for unit unmet demand of *o*-freight at node $j \in \mathcal{N}_\mathrm{D}$. The instance size is varied by adjusting the number of OD nodes (i.e., $|\mathcal{N}_\mathrm{O}|$ and $|\mathcal{N}_\mathrm{D}|$) and demand volume to reflect market fluctuations. The selection of OD nodes (i.e., cities) in China is based on the ranking of throughput volume in 2019. Note that demand matrix D represents the demand volume during a specific period (e.g., one week), correspondingly, the capacity of nodes and links indicates the upper bound of throughput during this period. Meanwhile, maintenance costs m^i_node and m^l_link correspond to the same period.

Although the effect of maintenance (e.g., dredging) for one element may last for several months, the maintenance cost of this element for a small time period (e.g., one week) could be calculated by means of division [54]. Furthermore, the parameter ε_i, describing the nonlinear relationship between maintenance cost and maintenance benefit in equation (1), is set to 1.8 and can be easily adjusted for specific cases. Notice that the calibration of maintenance-cost function is not the focus of this study.

(iii) *Budgeted uncertainty sets.* Regarding the specification of uncertainty budgets, we select the values of f_{node} and f_{link} from the range of 1 to 10. This range sufficiently encompasses the number of element failures across the majority of disruptive scenarios. Additionally, the partial-failure ratio α_i is confined to the interval [0,1]. As previously mentioned, element capacity, demand matrix, and maintenance cost pertain to the same time period, correspondingly, the impact of a failure is assumed to persist for the same period.

6.2. Benchmark solution method

The BD algorithm is used as the benchmark solution algorithm. Denote $\mathbf{y}$ as the first-stage decision and $(\mathbf{x},\mathbf{u})$ as the second-stage decision regarding the BVR model. The BD algorithm necessitates the dual information of the second-stage decision problem, for which we use $\boldsymbol{\lambda}$, $\boldsymbol{\mu}$, $\boldsymbol{\gamma}$, $\boldsymbol{\pi}$, and $\boldsymbol{\xi}$ to represent the corresponding dual variables. The dual subproblem $\mathcal{P}(\mathbf{y})$ can be formulated as a maximization problem over uncertainty set $\mathcal{D}$. To linearize the subproblem of the second-stage decision on $(\mathbf{x},\mathbf{u})$, we apply the big-M technique, resulting in the linearized dual subproblem $\mathcal{P}'(\mathbf{y})$ for the BD algorithm.

Due to the penalty cost incurred by unmet demand, an optimal solution $(\mathbf{z}_{\text{node}},\mathbf{z}_{\text{link}},\boldsymbol{\lambda},\boldsymbol{\mu},\boldsymbol{\gamma},\boldsymbol{\pi},\boldsymbol{\xi})$ to subproblem $\mathcal{P}'(\mathbf{y})$ can be obtained for any given $\mathbf{y}$ in each iteration. Subsequently, a cutting plane (47) is generated and incorporated into the MP, which is then solved to yield an optimal solution $(\mathbf{y}_{\text{node}},\mathbf{y}_{\text{link}},\phi)$. Notice that $\sum_{i\in\mathcal{N}_{\text{T}}} e_{y^i_{\text{node}}} + \sum_{(i,j)\in\mathcal{L}} e_{y^{(i,j)}_{\text{link}}} + \phi$ and $\sum_{i\in\mathcal{N}_{\text{T}}} e_{y^i_{\text{node}}} + \sum_{(i,j)\in\mathcal{L}} e_{y^{(i,j)}_{\text{link}}} + \mathcal{P}(\mathbf{y})$ provide the lower bound and upper bound, respectively, for the optimal value of the original problem.

By iteratively adding cutting plane (47) and solving the MP, the lower and upper bounds converge. Ultimately, an optimal solution for the original problem is determined.

6.3. Performance of solution methods

In this subsection, we evaluate the efficacy of the C&CG algorithms compared with the benchmark algorithm BD. Moreover, we delve into an analytical comparison of basic VA&R models, multi-set VA&R models, and SP-based VA&R models. For our numerical experiments, we set the optimality tolerance for termination at 10^{-4} and impose a computation time limit of 7,200 seconds. Upon reaching this time limit, the ongoing iteration is permitted to finish. It is pertinent to highlight that the SP-based VA&R models demand considerable computational time, thus, to facilitate a more equitable comparison with the basic VA&R models, we opt not to constrain their computational time. Each instance is labeled as "*NumONode-NumDNode-demand*", where *NumONode* and *NumDNode* represent the numbers of origin and destination nodes, respectively, and *demand* indicates the demand volume, expressed as a percentage (e.g., 80%, 100%, 120%) of the standard demand volume, offering insights into market fluctuation.

6.3.1. Application and performance

For the basic VA&R models, we limit the maximum number of disrupted nodes or links at three (i.e., $f_{\text{node}} = 3$ and $f_{\text{link}} = 3$), which covers most disruptive scenarios. In Table 3, the results in columns *DM* and *BVA model* are obtained using DM and BVA model, respectively. Column *Normal cost* shows the sum of transit costs and unmet-demand penalty costs in disruption-free situation, column *Time* indicates the computation time in seconds, column *Worst cost* displays the sum of transit costs and unmet-demand penalty costs in the worst disruptive scenario without maintenance in advance, and column *Rate* presents the vulnerability rate calculated by objective function (3). From Table 3, as expected, the normal cost (including transit costs of freight and penalty costs for unmet demand) in disruption-free situation increases accounting for a larger demand, and the increasing trend is illustrated quantitatively. When evaluating the IFTN vulnerability under different OD quantities and demand volumes, it is evident that IFTN vulnerability increases with the transportation burden. The varying vulnerability across different conditions can be assessed quantitatively. It is worth noting that when the

IFTN is subjected to the same disruptive scenario, the cost increase is more significant in high-demand scenarios compared to their low-demand counterparts. These results demonstrate that the IFTN is more sensitive to disruptions when it bears a larger transportation burden. Moreover, cascading failures are characterized by the maximization operation over the uncertainty set in objective function (3), which makes key alternative elements tend to fail and thus results in a worse cost. Specifically, when one element fails, alternative elements step in, leading the key alternative elements to potentially operate at their maximal capacity over extended durations, rendering them more susceptible to failure [57]. It is worth noting that the number of element failures remains respecting the predefined uncertainty-set budgets f_{node} and f_{link}.

Table 3. Vulnerability assessment using the BVA model.

Instance	DM		BVA model		
	Normal cost	Time (s)	Worst cost	Time (s)	Rate
10-10-80%	24,957,685.16	445.13	37,495,853.17	60.12	0.5024
10-10-100%	28,222,520.61	550.08	45,165,245.09	73.37	0.6003
10-10-120%	30,641,787.96	704.82	49,552,080.42	91.59	0.6171
15-15-80%	33,735,817.54	774.75	56,687,742.49	101.95	0.6803
15-15-100%	36,286,549.47	979.35	62,986,968.80	121.26	0.7358
15-15-120%	38,369,777.09	1,185.81	68,786,637.52	148.63	0.7927
20-20-80%	41,399,963.76	1,324.73	76,299,992.88	165.37	0.8430
20-20-100%	43,508,082.41	1,665.24	81,877,401.28	197.99	0.8819
20-20-120%	45,014,127.44	2,082.42	89,903,466.60	245.62	0.9972
25-25-80%	46,860,756.60	2,323.57	95,884,089.87	276.57	1.0461
25-25-100%	48,292,551.22	2,963.04	101,346,194.36	330.70	1.0986
25-25-120%	49,322,623.64	3,642.46	113,723,690.86	401.19	1.3057
Average	38,884,353.57	1,553.45	73,309,113.61	184.53	0.8418

In Table 4, the results in columns *BD*, *C&CG (1 thread)*, *C&CG*, and *C&CG Vary* are calculated by BD algorithm, C&CG algorithm with one thread without speedup strategies, C&CG algorithm with all threads without speedup strategies, and C&CG algorithm with all threads and the varying strategies in Section 5.2, respectively. Specifically, the C&CG (1 thread) algorithm is executed with Gurobi's thread parameter set to one, thus operating on a single thread; in contrast, the other algorithms employ Gurobi's default thread setting, allowing the utilization of all available threads. Further column *Iter* indicates the number of iterations until termination, column *Time* reports the computation time in seconds, column *UB* presents the best upper bound identified, and column *Gap* is calculated by (*UB*-*LB*)/*LB* at the computation termination. The insights from Table 4 reveal that the C&CG Vary algorithm significantly outperforms the BD algorithm in both computation time and iteration numbers. Particularly, the BD algorithm can only identify optimal solutions for two instance settings within the computation time limit, whereas the C&CG Vary algorithm succeeds in doing so for all instance settings. Therefore, the C&CG Vary algorithm exhibits superior solution quality within the computation time limit compared to the BD algorithm. For a more visual representation of the C&CG Vary algorithm's efficiency, convergence curves of the C&CG Vary algorithm and BD algorithm are compared in Figure 5, using instance 25-25-120% as a representative example. The convergence curve of the BD algorithm displays a slow decrease in the gap between lower and upper bounds. Even after 900 iterations, the gap fails to reach zero as the computation time limit is reached. In contrast, the C&CG Vary algorithm achieves optimality after only 12 iterations. Apart from the BD algorithm, the C&CG Vary algorithm also outperforms the C&CG (1 thread) and C&CG algorithms. Thus, the C&CG Vary algorithm is employed to solve instances for model comparison and sensitivity analysis in subsequent sections.

Table 4. Performance of different algorithms for the BVR model.

Instance	BD				C&CG (1 thread)				C&CG				C&CG Vary			
	Iter	Time (s)	UB	Gap (%)	Iter	Time (s)	UB	Gap (%)	Iter	Time (s)	UB	Gap (%)	Iter	Time (s)	UB	Gap (%)
10-10-80%	32	4,065.52	32,615,717.95	0.00	19	3,279.36	32,615,717.95	0.00	14	2,649.28	32,615,717.95	0.00	3	249.20	32,615,717.95	0.00
10-10-100%	82	6,926.43	37,139,584.04	0.00	25	3,924.59	37,139,584.04	0.00	17	3,130.64	37,139,584.04	0.00	3	280.72	37,139,584.04	0.00
10-10-120%	127	7,203.10	44,398,630.71	0.66	34	4,455.09	44,106,126.91	0.00	21	3,687.61	44,106,126.91	0.00	4	335.32	44,106,126.91	0.00
15-15-80%	171	7,213.28	47,859,314.07	0.88	42	4,881.85	47,441,604.40	0.00	25	3,874.20	47,441,604.40	0.00	5	355.56	47,441,604.40	0.00
15-15-100%	222	7,247.62	53,416,303.43	1.11	51	5,726.92	52,827,313.37	0.00	30	4,658.56	52,827,313.37	0.00	5	405.10	52,827,313.37	0.00
15-15-120%	295	7,212.23	59,807,966.37	1.40	60	6,804.14	58,984,094.07	0.00	36	5,372.81	58,984,094.07	0.00	6	469.26	58,984,094.07	0.00
20-20-80%	373	7,214.84	64,400,373.92	1.67	66	7,126.35	63,343,095.64	0.00	41	5,800.93	63,343,095.64	0.00	6	502.17	63,343,095.64	0.00
20-20-100%	442	7,219.35	71,779,621.22	2.01	72	7,207.47	70,389,807.62	0.03	46	6,810.65	70,367,612.77	0.00	7	576.80	70,367,612.77	0.00
20-20-120%	536	7,284.79	77,569,438.28	2.36	80	7,277.51	75,809,126.04	0.04	52	7,141.18	75,778,330.21	0.00	8	664.82	75,778,330.21	0.00
25-25-80%	729	7,216.65	83,660,837.66	2.92	86	7,267.13	81,333,313.71	0.06	58	7,209.43	81,311,036.49	0.03	9	717.38	81,287,874.22	0.00
25-25-100%	971	7,235.27	90,213,939.28	3.45	93	7,211.20	87,269,103.40	0.07	66	7,266.95	87,238,552.42	0.04	10	846.80	87,206,624.78	0.00
25-25-120%	975	7,259.16	97,144,217.13	3.54	103	7,270.57	93,916,225.79	0.10	75	7,273.48	93,890,727.82	0.07	12	969.84	93,821,610.95	0.00
Average	412.92	6,941.52	63,333,828.67	1.6670	60.92	6,036.02	62,097,926.08	0.0250	40.08	5,406.31	62,086,983.01	0.0116	6.50	531.08	62,076,632.44	0.00

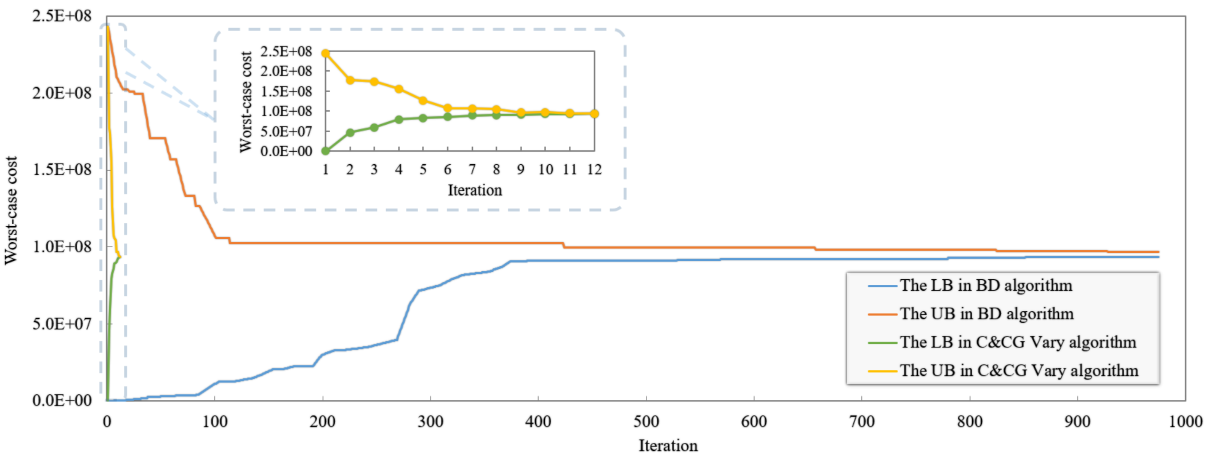

Figure 5. Convergence curves of the solution algorithms.

6.3.2. Model comparison and analyses

We compare and analyze the performance of three types of VA&R models, namely, basic VA&R models, multi-set VA&R models, and SP-based VA&R models.

6.3.2.1. Comparison of basic VA&R models and multi-set VA&R models

The experimental setting for each model is as follows. (i) For basic VA&R models, there is only one uncertainty set with $f_{\text{node}} = 3$ and $f_{\text{link}} = 3$. (ii) For multi-set VA&R models, there are four uncertainty sets $\mathcal{D}_0$, $\mathcal{D}_1$, $\mathcal{D}_2$, and $\mathcal{D}_3$. Set $\mathcal{D}_0$ represents the disruption-free situation, set $\mathcal{D}_1$ represents the scenario where exactly one node and one link fail, set $\mathcal{D}_2$ represents the scenario where exactly two nodes and two links fail, and set $\mathcal{D}_3$ represents the scenario where exactly three nodes and three links fail. We consider two weight settings, namely, (i) $\rho_0 = 0.55$, $\rho_1 = 0.20$, $\rho_2 = 0.15$, and $\rho_3 = 0.10$, where the IFTN is expected to be undisturbed in most cases, and (ii) $\rho_0 = 0.25$, $\rho_1 = 0.35$, $\rho_2 = 0.25$, and $\rho_3 = 0.15$, where the IFTN is more prone to disruptions.

Table 5 presents the comparison results between the BVA and MVA models. Column *Worst cost* shows the sum of transit costs and unmet-demand penalty costs in the worst disruptive scenario, column *Time* shows the computation time in seconds, and column *Rate* shows the vulnerability assessment according to objective functions (3) and (9), respectively. We found that the MVA model is less vulnerable than the BVA model. This is because the BVA model considers only one uncertainty set with $f_{\text{node}} = 3$ and $f_{\text{link}} = 3$, and imposes weight 1 on this set. In contrast, the MVA model imposes a lower weight on the uncertainty set with $f_{\text{node}} = 3$ and $f_{\text{link}} = 3$, and considers other uncertainty sets with fewer disruptions. This indicates the advantage of using multiple uncertainty sets with different disruption levels in the MVA model, according to decision-makers' experience and attitudes, rather than relying on only one uncertainty set with a high disruption level. This approach provides non-conservative solutions to decision-makers.

Table 5. Comparison of the BVA and MVA models.

Instance	BVA model			MVA model					
				ρ_0=0.55, ρ_1=0.20, ρ_2=0.15, ρ_3=0.10			ρ_0=0.25, ρ_1=0.35, ρ_2=0.25, ρ_3=0.15		
	Worst cost	Time (s)	Rate	Worst cost	Time (s)	Rate	Worst cost	Time (s)	Rate
10-10-80%	37,495,853.17	60.12	0.5024	27,879,806.06	207.98	0.1171	30,344,268.68	211.54	0.2158
10-10-100%	45,165,245.09	73.37	0.6003	32,258,416.45	261.46	0.1430	35,522,191.59	265.46	0.2586
10-10-120%	49,552,080.42	91.59	0.6171	35,165,169.22	315.01	0.1476	38,798,025.94	320.63	0.2662
15-15-80%	56,687,742.49	101.95	0.6803	39,283,997.89	354.23	0.1645	43,638,909.76	368.13	0.2935
15-15-100%	62,986,968.80	121.26	0.7358	42,786,810.97	444.26	0.1791	47,829,418.15	461.15	0.3181
15-15-120%	68,786,637.52	148.63	0.7927	45,832,711.57	548.25	0.1945	51,525,480.12	565.44	0.3429
20-20-80%	76,299,992.88	165.37	0.8430	50,029,985.80	585.14	0.2085	56,507,090.50	617.03	0.3649
20-20-100%	81,877,401.28	197.99	0.8819	53,041,697.19	744.60	0.2191	60,132,238.07	777.84	0.3821
20-20-120%	89,903,466.60	245.62	0.9972	56,266,052.07	918.26	0.2500	64,482,266.70	967.81	0.4325
25-25-80%	95,884,089.87	276.57	1.0461	59,203,084.05	1,018.79	0.2634	68,126,943.94	1,086.88	0.4538

25-25-100%	101,346,194.36	330.70	1.0986	61,697,080.94	1,237.68	0.2776	71,332,334.17	1,325.36	0.4771
25-25-120%	113,723,690.86	401.19	1.3057	65,736,206.15	1,552.86	0.3328	77,314,922.43	1,671.06	0.5675
Average	73,309,113.61	184.53	0.8418	47,431,751.53	682.38	0.2081	53,796,174.17	719.86	0.3644

Table 6 presents the comparison results between the BVR and MVR models. Column *Iter* shows the number of iterations; column *Worst cost* reports the sum of maintenance costs, transit costs of freight, and penalty costs of unmet demand; column *NodeN* reports the number of maintained nodes; column *LinkN* reports the number of maintained links; and column *Time* presents the computation time in seconds. We found that the solution to the BVR model is more conservative than the solution to the MVR model, as evidenced by the higher number of maintained nodes and links in the former. This is because the BVR model hedges against more disruptive scenarios in the uncertainty set and thus maintains more elements at a higher cost. For the larger weight on uncertainty sets in the MVR model, an increment in cost is expected compared with the lower weight on uncertainty sets in the MVR model. Nevertheless, the cost is still lower than the cost of the BVR model. Although the computation time of the MVR model is larger than that of the BVR model, the MVR model can still be solved to optimality in a reasonable time. Moreover, the use of multiple uncertainty sets and associated weights can effectively characterize the experience and maintenance attitudes of decision-makers. Overall, our analyses suggest that the multi-set VA&R models provide decision-makers with non-conservative and cost-effective solutions, adeptly capturing various levels of disruption hazards within the IFTN.

Table 6. Comparison of the BVR and MVR models.

Instance	BVR model					MVR model											
						ρ_0=0.55, ρ_1=0.20, ρ_2=0.15, ρ_3=0.10						ρ_0=0.25, ρ_1=0.35, ρ_2=0.25, ρ_3=0.15					
	Iter	Worst cost	NodeN	LinkN	Time (s)	Iter	Worst cost	NodeN	LinkN	Time (s)	Worst cost gap(%)	Iter	Worst cost	NodeN	LinkN	Time (s)	Worst cost gap(%)
10-10-80%	3	32,615,717.95	5	6	249.20	11	26,948,188.01	3	4	876.42	17.3767	12	27,399,200.14	4	5	889.07	15.9939
10-10-100%	3	37,139,584.04	7	9	280.72	13	30,043,578.30	4	5	1,011.83	19.1063	14	30,582,847.48	5	7	1,050.91	17.6543
10-10-120%	4	44,106,126.91	8	11	335.32	14	35,076,497.17	5	6	1,169.27	20.4725	16	35,868,190.29	6	8	1,220.79	18.6775
15-15-80%	5	47,441,604.40	8	12	355.56	16	37,358,978.64	5	8	1,303.48	21.2527	17	38,150,664.55	6	10	1,334.39	19.5839
15-15-100%	5	52,827,313.37	9	15	405.10	19	40,674,987.03	6	11	1,505.41	23.0039	20	41,632,782.48	7	13	1,563.40	21.1908
15-15-120%	6	58,984,094.07	10	17	469.26	21	44,544,815.48	7	13	1,725.69	24.4800	22	45,747,379.04	8	14	1,763.77	22.4412
20-20-80%	6	63,343,095.64	11	18	502.17	23	47,236,072.62	9	15	1,879.64	25.4282	24	48,522,903.97	10	16	1,953.95	23.3967
20-20-100%	7	70,367,612.77	13	21	576.80	28	50,656,546.55	10	18	2,198.82	28.0116	29	52,223,926.67	11	19	2,304.04	25.7841
20-20-120%	8	75,778,330.21	14	23	664.82	32	53,226,016.26	11	20	2,476.79	29.7609	34	55,002,134.21	12	21	2,689.96	27.4171
25-25-80%	9	81,287,874.22	15	25	717.38	35	56,058,706.67	12	22	2,751.58	31.0368	37	58,049,515.39	13	24	2,888.34	28.5877
25-25-100%	10	87,206,624.78	17	29	846.80	41	58,728,613.11	14	26	3,169.90	32.6558	43	60,933,063.26	15	28	3,339.35	30.1279
25-25-120%	12	93,821,610.95	18	32	969.84	46	61,253,265.94	15	29	3,580.76	34.7131	49	63,779,724.56	17	30	3,938.51	32.0202
Average	6.50	62,076,632.44	11.25	18.17	531.08	24.92	45,150,522.15	8.42	14.75	1,970.80	25.6082	26.42	46,491,027.67	9.50	16.25	2,078.04	23.5730

6.3.2.2. Comparison of multi-set VA&R models and SP-based VA&R models

We compare multi-set VA&R models and SP-based VA&R models through numerical experiments. In multi-set VA&R models, we adopt the uncertainty sets in Section 6.3.2.1, with the weights of sets

$\mathcal{D}_0$, $\mathcal{D}_1$, $\mathcal{D}_2$, and $\mathcal{D}_3$ being $\rho_0 = 0.43$, $\rho_1 = 0.37$, $\rho_2 = 0.16$, and $\rho_3 = 0.04$, respectively. In SP-based VA&R models, we set the failure probability of each node and link to be 0.01 and 0.001313, respectively, which closely match the weights of each uncertainty set in multi-set VA&R models: the probability of a disruption-free situation is about 0.426, the probability of exactly one node and one link being disrupted is about 0.365, the probability of exactly two nodes and two links being disrupted is about 0.155, and the probability of exactly three nodes and three links being disrupted is about 0.044.

Specifically, SP-based VA&R models consist of SP-based vulnerability assessment (SPVA) model and SP-based vulnerability reduction (SPVR) model. As shown in Table 7, the MVA model exhibits higher sensitive to vulnerability in comparison with the SPVA model. This difference stems from the MVA model's emphasis on the most adverse disruptive scenario within each uncertainty set. In contrast, the SPVA model considers a broader range of potential scenarios. Consequently, the vulnerability rate identified by the MVA model exceeds that determined by the SPVA model. It is worth noting that this discrepancy in vulnerability rates becomes increasingly evident as the OD quantity or demand volume increases. Table 8 further reveals that the total cost of the MVR model, including maintenance costs, transit costs, and unmet-demand penalty costs, is higher than that of the SPVR model. Particularly, the numbers of maintained nodes and links by the MVR model are larger than that by the SPVR model. Combining the insights from both Table 7 and Table 8, we conclude that multi-set VA&R models are not conservative in comparison with SP-based VA&R models. Moreover, it is noteworthy that the computation time of multi-set VA&R models is significantly shorter than that of SP-based VA&R models.

Table 7. Comparison of the MVA and SPVA models.

Instance	MVA model			SPVA model			Rate gap (%)
	Worst cost	Time (s)	Rate	Worst cost	Time (s)	Rate	
10-10-80%	28,101,367.52	209.70	0.1260	26,335,348.38	701.33	0.0552	56.1905
10-10-100%	32,499,021.41	263.71	0.1515	30,041,935.08	903.58	0.0645	57.4257
10-10-120%	35,612,055.74	317.63	0.1622	32,715,853.40	1,185.66	0.0677	58.2614
15-15-80%	39,867,165.84	358.50	0.1817	36,250,275.54	1,320.56	0.0745	58.9983
15-15-100%	43,503,219.42	451.36	0.1989	39,207,336.63	1,736.71	0.0805	59.5274
15-15-120%	46,596,030.63	556.83	0.2144	41,681,943.34	2,312.03	0.0863	59.7481
20-20-80%	50,867,584.23	597.02	0.2287	45,187,543.84	2,626.67	0.0915	59.9913
20-20-100%	53,923,049.31	761.16	0.2394	47,643,787.11	3,317.24	0.0951	60.2757
20-20-120%	57,211,465.16	937.87	0.2710	49,829,710.94	4,434.97	0.1070	60.5166
25-25-80%	60,181,214.07	1,043.81	0.2843	52,083,829.27	4,971.56	0.1115	60.7809
25-25-100%	62,770,997.63	1,265.38	0.2998	53,959,245.46	6,541.57	0.1173	60.8739
25-25-120%	66,822,233.75	1,584.11	0.3548	56,104,505.33	8,582.39	0.1375	61.2458
Average	48,162,950.39	695.59	0.2261	42,586,776.19	3,219.52	0.0907	59.4863

Table 8. Comparison of the MVR and SPVR models.

Instance	MVR model				SPVR model				Worst cost gap (%)
	Worst cost	**NodeN**	**LinkN**	**Time (s)**	**Worst cost**	**NodeN**	**LinkN**	**Time (s)**	
10-10-80%	27,039,499.20	3	4	879.03	22,943,070.58	2	2	3,765.50	15.1498
10-10-100%	30,172,520.67	4	5	1,024.14	25,227,981.71	3	3	4,698.46	16.3876
10-10-120%	35,229,150.10	5	6	1,185.82	29,023,677.18	4	4	5,934.55	17.6146
15-15-80%	37,534,946.16	5	8	1,309.79	30,495,528.69	4	5	6,768.41	18.7543
15-15-100%	40,878,155.57	6	11	1,517.99	32,720,546.99	5	8	8,754.03	19.9559
15-15-120%	44,781,354.22	7	14	1,727.42	35,400,701.61	6	10	11,132.93	20.9477
20-20-80%	47,499,709.66	9	16	1,901.26	36,952,783.34	6	11	12,333.75	22.2042
20-20-100%	50,945,589.58	10	18	2,214.68	39,094,749.27	8	13	15,331.05	23.2618
20-20-120%	53,542,717.81	12	21	2,506.61	40,715,296.22	8	14	18,833.51	23.9574
25-25-80%	56,403,516.19	13	22	2,759.08	42,286,266.85	9	16	22,238.60	25.0290
25-25-100%	59,096,573.33	15	27	3,188.66	43,765,856.83	11	21	28,110.30	25.9418
25-25-120%	61,746,733.91	16	30	3,631.50	45,084,620.45	12	23	35,271.99	26.9846
Average	45,405,872.20	8.75	15.17	1,987.16	35,309,256.64	6.50	10.83	14,431.09	21.3491

In addition, we compare multi-set VA&R models and SP-based VA&R models with basic VA&R models. Figure 6 illustrates that the vulnerability rates of the BVA model increase with the number of OD nodes and demand, while the vulnerability rates of the MVA model and SPVA model increase at a slower rate. Moreover, under a particular network and demand setting, the vulnerability rates of the MVA model and the SPVA model are significantly lower than that of the BVA model, with the vulnerability rate of the SPVA model being lower than that of the MVA model. Furthermore, the computation times of the BVA model and MVA model are much shorter than that of the SPVA model, while the computation time of the MVA model is longer than that of the BVA model. Figure 7 shows that the worst-case costs of the BVR model, MVR model, and SPVR model increase with the increase in OD quantity and demand volume. Specifically, the worst-case cost of the BVR model increases more significantly than that of the other two models, while the worst-case cost of the SPVR model is lower than that of the MVR model. Similarly, the computation times of the BVR model and MVR model are much shorter than that of the SPVR model, while the computation time of the MVR model is longer than that of the BVR model but still acceptable.

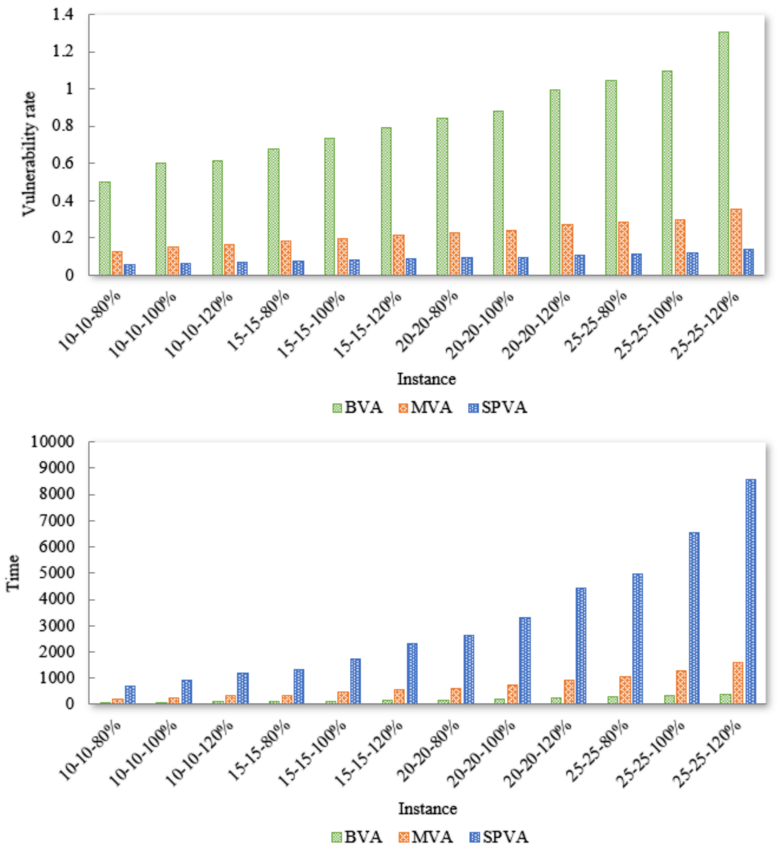

Figure 6. Comparison among the BVA, MVA, and SPVA models.

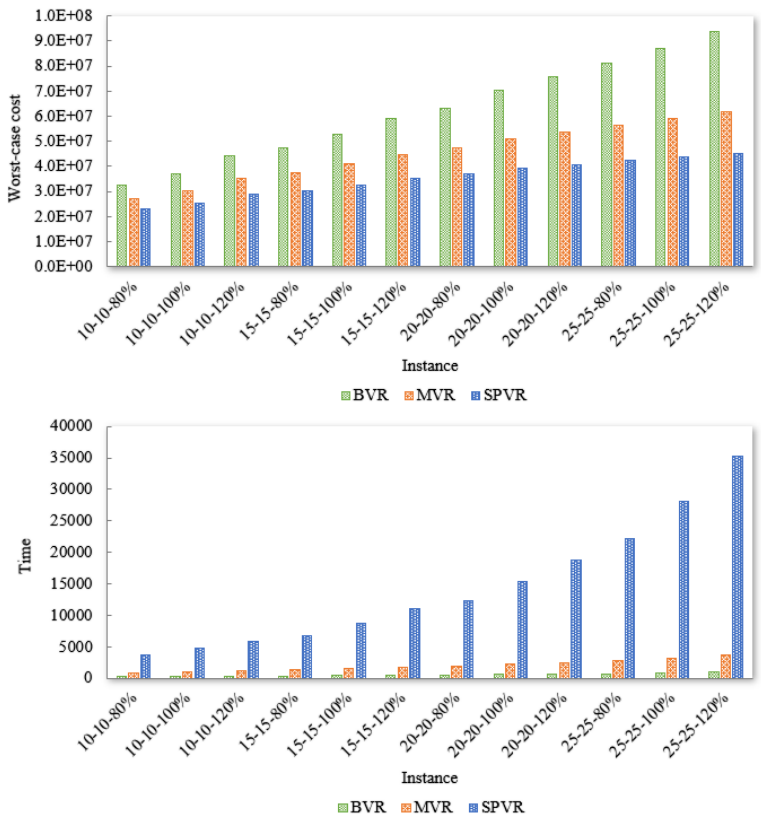

Figure 7. Comparison among the BVR, MVR, and SPVR models.

In summary, the findings from Figure 6 and Figure 7 suggest that multi-set VA&R models provide a balanced trade-off between disruption risk control and maintenance cost, while also accounting for diverse disruptive scenarios. Specifically, the vulnerability rate, worst-case cost (including maintenance costs, transit costs, and unmet-demand penalty costs), and computation time of the multi-set VA&R models fall between those of basic VA&R models and SP-based VA&R models. These observations support the two relationships: (i) when there is only one uncertainty set, multi-set VA&R models become basic VA&R models, and (ii) when each uncertainty set contains a single disruptive scenario, multi-set VA&R models resemble SP-based VA&R models. Thus, it can be inferred that multi-set VA&R models are a more practical solution that can offer a favorable balance between disruption risk management and maintenance cost control.

6.4. Sensitivity analysis

This work primarily concentrates on modeling and solution methods to address the VA&R problem for IFTNs. Furthermore, we investigate the impact of main parameters and provide managerial insights and practical references, by employing a comprehensive range of values for each main parameter.

6.4.1. Impact of disruptions and maintenance

The absence of maintenance results in significant recourse costs and unmet-demand penalty costs when disruptions occur. We have conducted numerical experiments for 12 instance settings to gain insights into the impact of disruption and maintenance, and the results are reported in Figure 8. Curve *DM (normal cost)* shows the sum of transit costs and unmet-demand penalty costs under disruption-free situation. Curve *BVA (worst cost)* shows the sum of transit costs and unmet-demand penalty costs under the worst disruptive scenario without maintenance. Curve *BVR (maintenance cost)* shows the cost of implementing maintenance decisions calculated by the BVR model, while curve *BVR (worst cost)* shows the total cost (including maintenance costs, transit costs, and unmet-demand penalty costs) under the worst disruptive scenario with maintenance decisions. The difference between *BVA (worst cost)* and *BVR (worst cost)* is represented by curve *Deviation*, which indicates the cost difference between implementing and not implementing maintenance. Curve *BVA (rate)* shows the vulnerability rate.

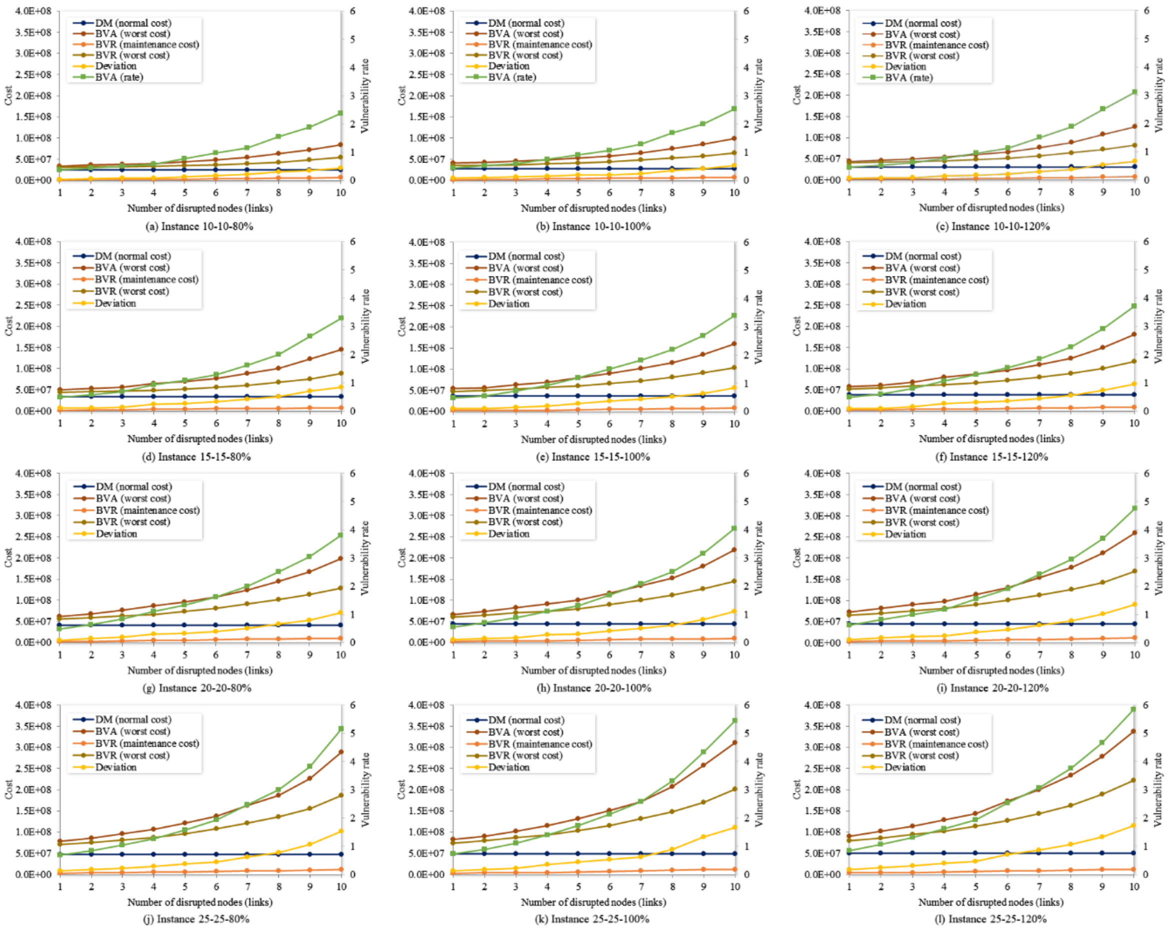

Figure 8. Impacts of disruptions and maintenance on the costs.

Under the disruption-free situation, as expected, the operation cost increases as the demand volume increases, given the OD remains unchanged. Analogously, the operation cost increases with the addition of OD nodes as additional demand volume is incurred by the added OD nodes. For example, comparing instances 10-10-80% and 10-10-120% reveals the impact of incremental demand volume, while comparing instances 10-10-80% and 25-25-80% illustrates the impact of incremental OD node quantity and the corresponding demand volume associated with the newly incorporated OD nodes. For a particular instance setting, such as 10-10-80%, it is observed that the values of *BVA (worst cost)*, *BVR (maintenance cost)*, *BVR (worst cost)*, *Deviation*, and *BVA (rate)* increase as the number of disrupted elements increased. These results quantitatively showed that considering disruptions generates maintenance costs in the first stage, however, ignoring disruptions will result in higher costs when disruptions occur. Moreover, the cost difference between considering and not considering maintenance significantly increases with the number of OD nodes and demand volume. This demonstrates the advantage of considering maintenance, especially for high-demand IFTNs. Moreover, the maintenance cost is related to the uncertainty-set budgets (i.e., f_{node} and f_{link}). The maintenance cost is around 6% of the disruption-free operation cost when the values of f_{node} and f_{link} are both less than three, which cover most disruptive scenarios in practice. Overall, the vulnerability rate increases with increasing demand volume, OD nodes, and uncertainty-set budgets; the sensitivity of vulnerability rate to these three factors can be quantitatively observed; and the BVR model significantly reduces recourse costs at a small maintenance cost.

6.4.2. Impact of uncertainty-set weights

The weights of uncertainty sets reflect the experience and maintenance attitudes of decision-makers. To gain insights into the impact of these weights, we conducted numerical experiments for 12 instance settings, varying the number of OD nodes from 10 to 25 and demand volume from 80% to 120% of the standard demand. For each instance setting, we considered two uncertainty sets: set $\mathcal{D}_1$ with $f_{\text{link}} = f_{\text{node}} = 0$ (i.e., no disruption), and set $\mathcal{D}_2$ with $f_{\text{link}} = f_{\text{node}} = 2$, 3, or 4 (referred to as $f = 2$, 3, or 4). We gradually vary the weight values and report the results in Figure 9 (impact on vulnerability rates) and Figure 10 (impact on costs), respectively.

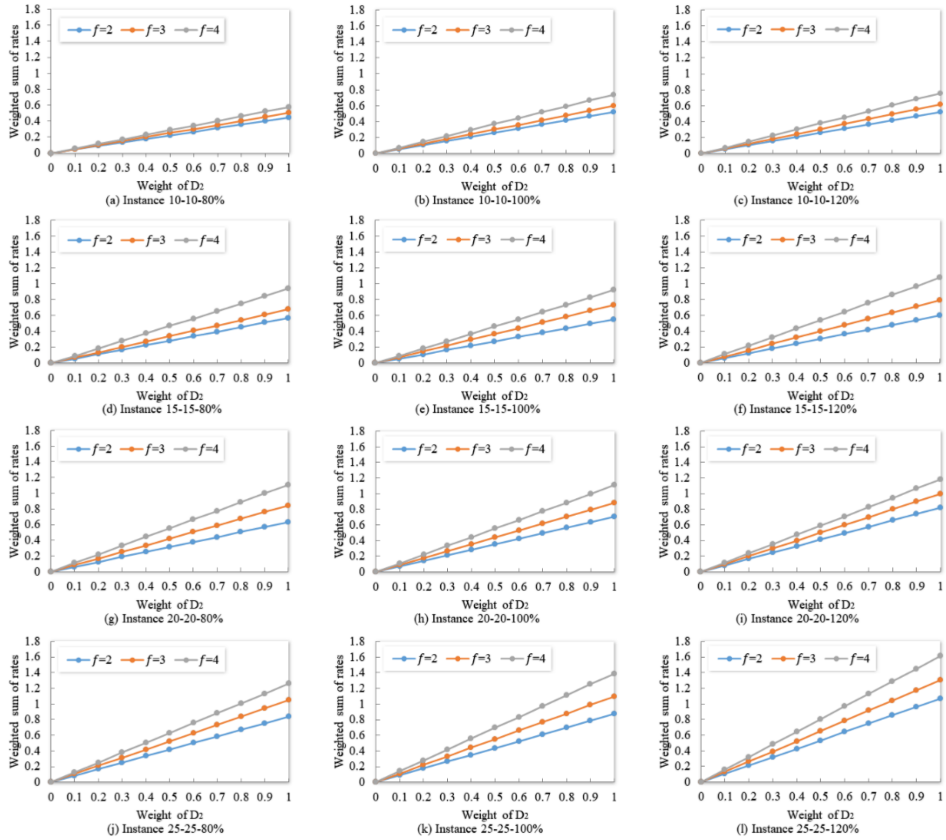

Figure 9. Impact of uncertainty-set weights on the vulnerability rates.

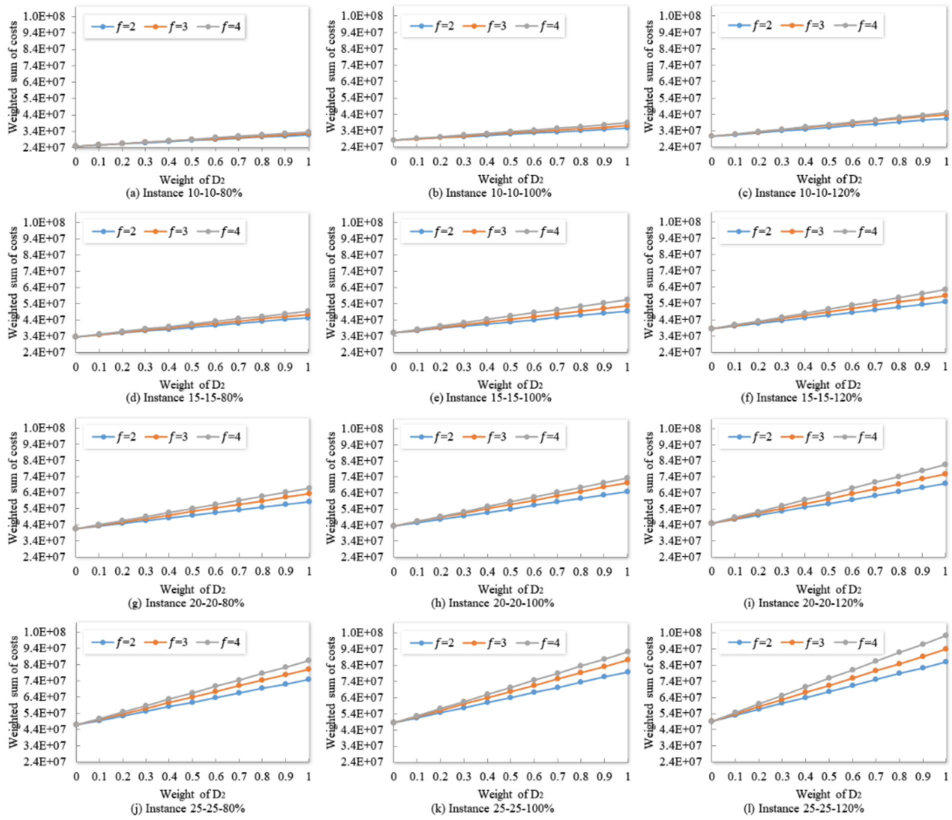

Figure 10. Impact of uncertainty-set weights on the costs.

Our results illustrate that the objective values of the multi-set VA&R models increase as the weight of set $\mathcal{D}_2$ becomes larger, indicating that the worst disruptive scenario in set $\mathcal{D}_2$ largely affects the vulnerability rate and worst-case cost. Figure 9 shows that the relationship between the vulnerability rate and the weight is basically linear. Moreover, at each weight value, the difference between curve $f = 3$ and curve $f = 4$ is larger than the difference between curve $f = 2$ and curve $f = 3$. This quantitative finding reveals that with an increasing number of disrupted elements, the impact of each newly disrupted element is larger, and the importance of the remaining elements increases. In Figure 10, the relationship between cost and weight value is basically linear. However, the difference between curve $f = 3$ and curve $f = 4$ is usually smaller than the difference between curve $f = 2$ and curve $f = 3$ on average, which is different from the difference changes in Figure 9. This is due to the maintenance considered in BVR model, and thus reflects the impact and advantage of maintenance decisions. When $f = 2$, vulnerability rates and costs are less sensitive to the weight, compared with settings $f = 3$ and $f = 4$. Therefore, uncertainty sets with larger budgets should be weighed carefully for disruptive scenario settings, whereas for a small-budget uncertainty set, errors in weight may not incur a significant influence on vulnerability rates and costs.

6.4.3. Impact of partial failure and uncertainty-set budgets

The vulnerability rates and worst-case costs of IFTNs are influenced by both partial failures and uncertainty-set budgets (i.e., f_{node} and f_{link}). However, the extent of this impact remains to be determined. Therefore, we investigate the coupling impact of partial failures and uncertainty-set budgets. To conserve space, we present numerical experiments for two representative instance settings (instances 10-10-80% and 25-25-120%), where we simultaneously vary the degree of partial failure and uncertainty-set budget. The results are reported in Figure 11 and Figure 12. Particularly, Figure 11 shows the impact of the parameters α, f_{node}, and f_{link} on vulnerability rates, and Figure 12 shows their impact on worst-case costs. We observe that both vulnerability rates and worst-case costs increase as the uncertainty-set budget increases, irrespective of the presence of complete or partial failures. Specifically, when the degree of partial failure is small (e.g., no greater than 0.2), the variation in both vulnerability rates and worst-case costs is minimal despite significant changes in the uncertainty-set budget. This is because the remaining capacity of disrupted elements can still meet the transportation demand. However, when the degree of partial failure is large (e.g., greater than 0.4), an increase in the uncertainty-set budget has a noticeable impact on both vulnerability rates and worst-case costs. Importantly, this impact increases significantly with an increase in the degree of partial failure. Based on these findings, in regions where small disruptions are anticipated, we recommend that decision-makers consider uncertainty sets with larger uncertainty-set budgets for better disruption risk control. This would not incur a significant increase in maintenance costs. However, when the degree of partial failure is likely to exceed 0.4, decision-makers should exercise caution when setting uncertainty-set budgets, as the cost of network maintenance becomes more sensitive to the uncertainty-set budget.

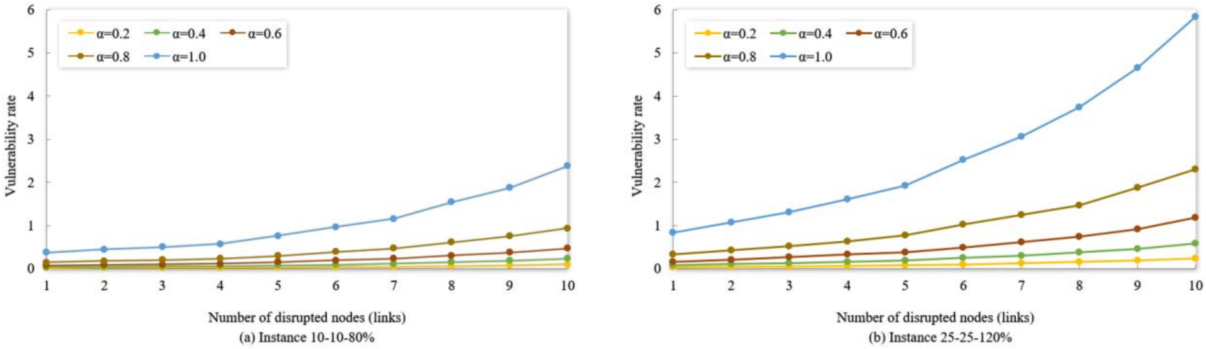

Figure 11. Impact of parameters α, f_{node}, and f_{link} on vulnerability rates.

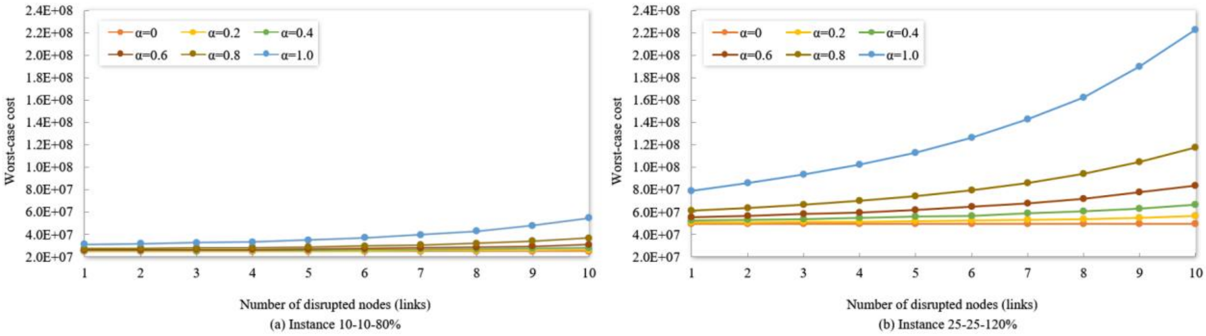

Figure 12. Impact of parameters α, f_{node}, and f_{link} on worst-case costs.

6.4.4. Insights on critical nodes and links

In our examination of the IFTN, the identification of critical nodes and links plays an instrumental role. Based on extensive numerical experiments and sensitivity analyses under varied scenarios, insights are achieved into critical elements in the IFTN, as depicted in Figure 2. Recognizing that some place names in the case study might be unfamiliar to a broad readership, this discussion focuses on presenting insights in a clear and instructive manner to avoid overly specific geographical references, thereby ensuring broader comprehensibility.

(i) Identification of critical nodes: (a) Major sea ports: Ports such as Shanghai, Singapore, and Antwerp are identified as critical nodes. Their strategic importance is underscored by their high cargo volumes and pivotal geographic positions in the network. (b) Key river ports: Within China, river ports like Chongqing and Wuhan along the Yangtze River are marked as critical. The importance of these river ports is underlined by their proximity to major industrial areas, high transportation volumes, and limited alternatives by other local transportation infrastructures. (c) Strategic railway junctions: Junctions such as Zhengzhou and Jinan in China's freight railway network are highlighted as key nodes. Their role in facilitating the efficient transfer of goods across different regions cements their critical status. (d) Important road intersections: Nodes like Beijing and Hefei in the road subnetwork are recognized as vital, owing to their role in flexibly distributing goods in the network.

(ii) Identification of critical links: (a) Maritime chokepoint segments: Segments along the westbound and eastbound sea routes, particularly those passing through strategic corridors like the Suez Canal, are deemed critical. These links, connecting regions with limited low-cost alternative links and handling large freight volumes, are pivotal for global freight flow. (b) Key river passages: River links, such as the one connecting Chongqing with Wuhan, are crucial due to their cost-effectiveness and capacity for transporting large volumes over a long distance, underscoring their significant role in the IFTN. (c) Vital railway links: Segments of China's main freight railways, especially those leading to international exits like the link from Changsha to Shenzhen, are identified as critical links of the network. (d) Critical road segments: Key road segments, such as the one linking Hangzhou to Shanghai, and those facilitating first/last-mile delivery with few alternative links, are recognized for their criticality. Their flexibility and timeliness, especially over short distances, make them integral to the network.

The identification of critical nodes and links considers multiple factors, including freight volume, network configuration (especially the availability of alternative elements), and the element's cost-effectiveness in the IFTN. These insights are crucial in guiding maintenance, namely, the identification of critical elements informs targeted efforts for vulnerability reduction to strengthen key components of the IFTN. Such strategic attention, akin to measures taken by authorities like the Suez Canal

Authority following the canal blockage incident in March 2021, is essential in enhancing the network's reliability, especially in the global freight transportation context.

7. Conclusions

In this study, we address VA&R for already-constructed IFTNs in the face of uncertain disruptions. We comprehensively consider a variety of main aspects: uncertain disruptions in both nodes and links, multiple budgeted uncertainty sets, complete and partial failures of network elements, interconnection and interdependence among network elements, cascading failures and influence spreading in IFTNs, and all the four prevalent transportation modes for IFTNs. Thus, we have characterized a diverse range of uncertain disruptive scenarios, considering practical operational features of IFTNs. Moreover, we have formulated basic and extended VA&R models utilizing two-stage robust optimization techniques. Furthermore, we build an exact solution method integrating the C&CG algorithm framework and speedup strategies. This solution method, tailored for the already-constructed IFTNs with unique problem features and model structure, can optimally solve the instances in a reasonable time. With in-depth numerical experiments on a real-world IFTN, managerial insights have been achieved to provide valuable references for practical operations.

Future research can potentially extend this work in two directions. First, while the current study emphasizes methods to assess and reduce vulnerability of IFTNs based on the original demand volume, it would be meaningful to examine changes in freight demand in the context of disruptive events. Second, even though our case study delves into a real-world international IFTN, there is value in pursuing extensive studies covering larger regions. Accordingly, heuristic algorithms can be developed to address the computational complexity of expansive IFTNs for more efficient solutions.

CRediT author statement

Xiaoyang Wei: Conceptualization, Methodology, Analysis and interpretation of results, Writing - Original draft preparation. **Mengtong Wang:** Analysis and interpretation of results, Writing - Reviewing and editing. **Qiang Meng:** Conceptualization, Methodology, Writing - Reviewing and editing, Supervision, Project administration.

Declaration of competing interest

The authors declare that they have no known competing interests regarding the work reported in this paper.

Acknowledgments

This study is supported by the research project “Analysis of intermodal container transport network in the context of Chongqing Connectivity Initiative - International Land-Sea Trade Corridor (CCI-ILSTC) and China - Singapore / ASEAN region” (SMI-2020-MA-05) funded by Singapore Maritime Institute. Any opinions, findings, conclusions, or recommendations expressed in this paper are those of the author(s) and do not reflect the views of Singapore Maritime Institute.

Appendices

Appendix A. Deterministic model

[DM]:

$$\min \sum_{(i,j)\in\mathcal{L}} \sum_{o\in\mathcal{N}_\mathrm{O}} c_{(i,j)} x_{(i,j)}^{o} + \sum_{j\in\mathcal{N}_\mathrm{D}} \sum_{o\in\mathcal{N}_\mathrm{O}} \theta_j^o u_j^o \tag{A1}$$

$$\text{s.t.} \sum_{j\in\mathcal{N}_o^+} x_{(o,j)}^{o} \le v_o \quad \forall o\in\mathcal{N}_\mathrm{O} \tag{A2}$$

$$\sum_{j\in\mathcal{N}_i^-} x_{(j,i)}^{o} = \sum_{j\in\mathcal{N}_i^+} x_{(i,j)}^{o} \quad \forall o\in\mathcal{N}_\mathrm{O},\ i\in\mathcal{N}_\mathrm{T} \tag{A3}$$

$$\sum_{i\in\mathcal{N}_j^-} x_{(i,j)}^{o} + u_j^o = v_j^o \quad \forall o\in\mathcal{N}_\mathrm{O},\ j\in\mathcal{N}_\mathrm{D} \tag{A4}$$

$$\sum_{j\in\mathcal{N}_i^+} \sum_{o\in\mathcal{N}_\mathrm{O}} x_{(i,j)}^{o} \le q_\mathrm{node}^{i} \quad \forall i\in\mathcal{N}_\mathrm{T} \tag{A5}$$

$$\sum_{o\in\mathcal{N}_\mathrm{O}} x_{(i,j)}^{o} \le q_\mathrm{link}^{(i,j)} \quad \forall (i,j)\in\mathcal{L} \tag{A6}$$

$$x_{(i,j)}^{o} \ge 0 \quad \forall o\in\mathcal{N}_\mathrm{O},\ (i,j)\in\mathcal{L} \tag{A7}$$

$$u_i^o \ge 0 \quad \forall o\in\mathcal{N}_\mathrm{O},\ i\in\mathcal{N}_\mathrm{D} \tag{A8}$$

Objective function (A1) aims to minimize the sum of transit costs and unmet-demand penalty costs in the disruption-free scenario. Constraints (A2) - (A4) limit the freight flow for origin nodes ($\mathcal{N}_{\mathrm{O}}$), transit nodes ($\mathcal{N}_{\mathrm{T}}$), and destination nodes ($\mathcal{N}_{\mathrm{D}}$), respectively. Constraints (A5) and (A6) impose limits on the freight flow, taking into account the capacity of each individual node and link. Constraints (A7) and (A8) define the domain of decision variables.

Appendix B. SP-based VA&R models

The following notations are additionally needed to formulate SP-based VA&R models.

$\mathcal{A}$ Set of disruptive scenarios

p_a Occurrence probability of disruptive scenario $a \in \mathcal{A}$

$x^o_{(i,j)a}$ Volume of *o*-freight ($o \in \mathcal{N}_{\mathrm{O}}$) from node i to node j in disruptive scenario $a \in \mathcal{A}$

u^o_{ia} Volume of unmet demand for *o*-freight ($o \in \mathcal{N}_{\mathrm{O}}$) at node $i \in \mathcal{N}_{\mathrm{D}}$ in disruptive scenario $a \in \mathcal{A}$

z_{ia} Equals 1 if element $i \in \mathcal{N}_{\mathrm{T}} \cup \mathcal{L}$ is disrupted in scenario $a \in \mathcal{A}$, and 0 otherwise

SP-based VA&R models include SP-based vulnerability assessment (SPVA) model and SP-based vulnerability reduction (SPVR) model, which are formulated as follows.

[SPVA Model]:

$$\min \sum_{a \in \mathcal{A}} p_a \left(\sum_{(i,j) \in \mathcal{L}} \sum_{o \in \mathcal{N}_{\mathrm{O}}} c_{(i,j)} x^o_{(i,j)a} + \sum_{j \in \mathcal{N}_{\mathrm{D}}} \sum_{o \in \mathcal{N}_{\mathrm{O}}} \theta^o_j u^o_{ja} \right) / v_{\mathrm{DM}} - 1 \tag{B1}$$

$$\text{s.t.} \sum_{j \in \mathcal{N}^+_o} x^o_{(o,j)a} \le v_o \quad \forall a \in \mathcal{A}, o \in \mathcal{N}_{\mathrm{O}} \tag{B2}$$

$$\sum_{j \in \mathcal{N}^-_i} x^o_{(j,i)a} = \sum_{j \in \mathcal{N}^+_i} x^o_{(i,j)a} \quad \forall a \in \mathcal{A},\ o \in \mathcal{N}_{\mathrm{O}}, i \in \mathcal{N}_{\mathrm{T}} \tag{B3}$$

$$\sum_{i \in \mathcal{N}^-_j} x^o_{(i,j)a} + u^o_{ja} = v^o_j \quad \forall a \in \mathcal{A},\ o \in \mathcal{N}_{\mathrm{O}}, j \in \mathcal{N}_{\mathrm{D}} \tag{B4}$$

$$\sum_{j \in \mathcal{N}^+_i} \sum_{o \in \mathcal{N}_{\mathrm{O}}} x^o_{(i,j)a} \le \left(1 - z_{ia}\right) q^i_{\mathrm{node}} \quad \forall a \in \mathcal{A}, i \in \mathcal{N}_{\mathrm{T}} \tag{B5}$$

$$\sum_{o \in \mathcal{N}_{\mathrm{O}}} x^o_{(i,j)a} \le \left(1 - z_{(i,j)a}\right) q^{(i,j)}_{\mathrm{link}} \quad \forall a \in \mathcal{A}, (i,j) \in \mathcal{L} \tag{B6}$$

$$x^o_{(i,j)a} \ge 0 \quad \forall a \in \mathcal{A}, (i,j) \in \mathcal{L},\ o \in \mathcal{N}_{\mathrm{O}} \tag{B7}$$

$$u_{ia}^{o} \geq 0 \quad \forall a \in \mathcal{A},\ o \in \mathcal{N}_{\mathrm{O}}, i \in \mathcal{N}_{\mathrm{D}} \tag{B8}$$

[SPVR Model]:

$$\min \sum_{i \in \mathcal{N}_{\mathrm{T}}} e_{y_{\mathrm{node}}^{i}} + \sum_{(i,j) \in \mathcal{L}} e_{y_{\mathrm{link}}^{(i,j)}} + \sum_{a \in \mathcal{A}} p_a \left(\sum_{(i,j) \in \mathcal{L}} \sum_{o \in \mathcal{N}_{\mathrm{O}}} c_{(i,j)} x_{(i,j)a}^{o} + \sum_{j \in \mathcal{N}_{\mathrm{D}}} \sum_{o \in \mathcal{N}_{\mathrm{O}}} \theta_j^o u_{ja}^{o} \right) \tag{B9}$$

s.t. (1), (B2) - (B4), (B7), (B8),

$$\sum_{j \in \mathcal{N}_i^+} \sum_{o \in \mathcal{N}_{\mathrm{O}}} x_{(i,j)a}^{o} \leq \left(1 - z_{ia}\left(1 - y_{\mathrm{node}}^{i}\right)\right) q_{\mathrm{node}}^{i} \quad \forall a \in \mathcal{A}, i \in \mathcal{N}_{\mathrm{T}} \tag{B10}$$

$$\sum_{o \in \mathcal{N}_{\mathrm{O}}} x_{(i,j)a}^{o} \leq \left(1 - z_{(i,j)a}\left(1 - y_{\mathrm{link}}^{(i,j)}\right)\right) q_{\mathrm{link}}^{(i,j)} \quad \forall a \in \mathcal{A}, (i,j) \in \mathcal{L} \tag{B11}$$

$$y_{\mathrm{node}}^{i} \in [0,1] \quad \forall i \in \mathcal{N}_{\mathrm{T}} \tag{B12}$$

$$y_{\mathrm{link}}^{(i,j)} \in [0,1] \quad \forall (i,j) \in \mathcal{L} \tag{B13}$$

References

[1] Wang X, Meng Q. Discrete intermodal freight transportation network design with route choice behavior of intermodal operators. Transp Res Part B: Methodol 2017;95:76–104.

[2] Basallo-Triana MJ, Vidal-Holguín CJ, Bravo-Bastidas JJ. Planning and design of intermodal hub networks: A literature review. Comput Oper Res 2021;136:105469.

[3] Mattsson LG, Jenelius E. Vulnerability and resilience of transport systems - A discussion of recent research. Transp Res Part A: Policy Pract 2015;81.

[4] Gu Y, Fu X, Liu Z, Xu X, Chen A. Performance of transportation network under perturbations: Reliability, vulnerability, and resilience. Transp Res Part E: Logist Trans Rev 2020;133.

[5] Huang W, Zhou B, Yu Y, Yin D. Vulnerability analysis of road network for dangerous goods transportation considering intentional attack: Based on Cellular Automata. Reliab Eng Syst Saf 2021;214:107779.

[6] Freitas S, Yang D, Kumar S, Tong H, Chau DH. Graph vulnerability and robustness: A survey. IEEE Trans Knowl Data Eng 2023;35:5915–34.

[7] Mahmoudzadeh A, Khodakarami M, Ma C, Mitchell KN, Wang XB, Zhang Y. Waterway

maintenance budget allocation in a multimodal network. Transp Res Part E: Logist Trans Rev 2021;146:102215.

[8] Zarghami SA, Dumrak J. Unearthing vulnerability of supply provision in logistics networks to the black swan events: Applications of entropy theory and network analysis. Reliab Eng Syst Saf 2021;215:107798.

[9] Chen A, Yang H, Lo HK, Tang WH. Capacity reliability of a road network: An assessment methodology and numerical results. Transp Res Part B: Methodol 2002;36:225–52.

[10] Scott DM, Novak DC, Aultman-Hall L, Guo F. Network robustness index: A new method for identifying critical links and evaluating the performance of transportation networks. J Transp Geogr 2006;14:215–27.

[11] Murray AT, Matisziw TC, Grubesic TH. Critical network infrastructure analysis: Interdiction and system flow. J Geogr Syst 2007;9:103–17.

[12] Peterson SK, Church RL. A framework for modeling rail transport vulnerability. Growth Change 2008;39:617–41.

[13] Santos BF, Antunes AP, Miller EJ. Interurban road network planning model with accessibility and robustness objectives. Transp Plan Technol 2010;33:297–313.

[14] Sullivan JL, Novak DC, Aultman-Hall L, Scott DM. Identifying critical road segments and measuring system-wide robustness in transportation networks with isolating links: A link-based capacity-reduction approach. Transp Res Part A: Policy Pract 2010;44:323–36.

[15] Jenelius E, Mattsson LG. Road network vulnerability analysis of area-covering disruptions: A grid-based approach with case study. Transp Res Part A: Policy Pract 2012;46.

[16] Gedik R, Medal H, Rainwater C, Pohl EA, Mason SJ. Vulnerability assessment and re-routing of freight trains under disruptions: A coal supply chain network application. Transp Res Part E: Logist Trans Rev 2014;71:45–57.

[17] Rodríguez-Núñez E, García-Palomares JC. Measuring the vulnerability of public transport networks. J Transp Geogr 2014;35:50–63.

[18] Khaled AA, Jin M, Clarke DB, Hoque MA. Train design and routing optimization for evaluating criticality of freight railroad infrastructures. Transp Res Part B: Methodol 2015;71:71–84.

[19] Stamos I, Mitsakis E, Salanova JM, Aifadopoulou G. Impact assessment of extreme weather events on transport networks: A data-driven approach. Transp Res Part D: Transp Environ 2015;34:168–78.

[20] Wang DZW, Liu H, Szeto WY, Chow AHF. Identification of critical combination of vulnerable links in transportation networks – a global optimisation approach. Transp Sci 2016;12:346–65.

[21] Bell MGH, Kurauchi F, Perera S, Wong W. Investigating transport network vulnerability by capacity weighted spectral analysis. Trans Res Part B: Methodol 2017;99.

[22] Cats O, Koppenol GJ, Warnier M. Robustness assessment of link capacity reduction for complex networks: Application for public transport systems. Reliab Eng Syst Saf 2017;167:544–53.

[23] Darayi M, Barker K, Santos JR. Component importance measures for multi-industry vulnerability of a freight transportation network. Netw Spat Econ 2017;17:1111–36.

[24] Whitman MG, Barker K, Johansson J, Darayi M. Component importance for multi-commodity networks: Application in the Swedish railway. Comput Ind Eng 2017;112:274–88.

[25] Zhou Y, Wang J. Critical link analysis for urban transportation systems. IEEE Trans Intell Transp Syst 2018;19:402–15.

[26] Szymula C, Bešinović N. Passenger-centered vulnerability assessment of railway networks. Transp Res Part B: Methodol 2020;136:30–61.

[27] He Z, Navneet K, van Dam W, Van Mieghem P. Robustness assessment of multimodal freight transport networks. Reliab Eng Syst Saf 2021;207:107315.

[28] Lu QC, Zhang L, Xu PC, Cui X, Li J. Modeling network vulnerability of urban rail transit under cascading failures: A Coupled Map Lattices approach. Reliab Eng Syst Saf 2022;221.

[29] Wen T, Gao Q, Chen Y wang, Cheong KH. Exploring the vulnerability of transportation networks by entropy: A case study of Asia–Europe maritime transportation network. Reliab Eng Syst Saf 2022;226.

[30] Zhang J, Min Q, Zhou Y, Cheng L. Vulnerability assessments of urban rail transit networks based on extended coupled map lattices with evacuation capability. Reliab Eng Syst Saf 2024;243:109826.

[31] Wen H, Ye Y, Zhang L. Optimizing road networks in underdeveloped regions for improving

comprehensive efficiency integrated by accessibility, vulnerability and socioeconomic interaction. Reliab Eng Syst Saf 2024;243:109848.

[32] Zhang Z, Li X, Li H. A quantitative approach for assessing the critical nodal and linear elements of a railway infrastructure. Int J Crit Infrastruct Prot 2015;8:3–15.

[33] Shanmukhappa T, Ho IWH, Tse CK. Spatial analysis of bus transport networks using network theory. Physica A 2018;502:295–314.

[34] Abedi A, Gaudard L, Romerio F. Review of major approaches to analyze vulnerability in power system. Reliab Eng Syst Saf 2019;183:153–72.

[35] Yap MD, van Oort N, van Nes R, van Arem B. Identification and quantification of link vulnerability in multi-level public transport networks: A passenger perspective. Transportation (Amst) 2018;45:1161–80.

[36] Abedi A, Gaudard L, Romerio F. Power flow-based approaches to assess vulnerability, reliability, and contingency of the power systems: The benefits and limitations. Reliab Eng Syst Saf 2020;201:106961.

[37] Bababeik M, Nasiri MM, Khademi N, Chen A. Vulnerability evaluation of freight railway networks using a heuristic routing and scheduling optimization model. Transportation (Amst) 2019;46:1143–70.

[38] Zio E. Reliability engineering: Old problems and new challenges. Reliab Eng Syst Saf 2009;94:125–41.

[39] Xie W, Ouyang Y, Wong SC. Reliable location-routing design under probabilistic facility disruptions. Transp Sci 2016;50:1128–38.

[40] Ben-Tal A, Nemirovski A. Robust solutions of linear programming problems contaminated with uncertain data. Math Program 2000;88:411–24.

[41] Ben-Tal A, Goryashko A, Guslitzer E, Nemirovski A. Adjustable robust solutions of uncertain linear programs. Math Program 2004;99:351–76.

[42] Atamtürk A, Zhang M. Two-stage robust network flow and design under demand uncertainty. Oper Res 2007;55:662–73.

[43] Bertsimas D, Brown DB, Caramanis C. Theory and applications of robust optimization. SIAM

Rev Soc Ind Appl Math 2011;53:464–501.

[44] Bertsimas D, Litvinov E, Sun XA, Zhao J, Zheng T. Adaptive robust optimization for the security constrained unit commitment problem. IEEE Trans Power Syst 2013;28:52–63.

[45] Zeng B, Zhao L. Solving two-stage robust optimization problems using a column-and- constraint generation method. Oper Res Lett 2013;41:457–61.

[46] An Y, Zeng B, Zhang Y, Zhao L. Reliable p-median facility location problem: Two-stage robust models and algorithms. Transp Res Part B: Methodol 2014;64:54–72.

[47] Cheng C, Qi M, Zhang Y, Rousseau LM. A two-stage robust approach for the reliable logistics network design problem. Transp Res Part B: Methodol 2018;111:185–202.

[48] An Y, Zhang Y, Zeng B. The reliable hub-and-spoke design problem: Models and algorithms. Transp Res Part B: Methodol 2015;77:103–22.

[49] An Y, Zeng B. Exploring the modeling capacity of two-stage robust optimization: Variants of robust unit commitment model. IEEE Trans Power Syst 2015;30:109–22.

[50] Wandelt S, Shi X, Sun X. Estimation and improvement of transportation network robustness by exploiting communities. Reliab Eng Syst Saf 2021;206.

[51] Wang N, Wu M, Yuen KF. A novel method to assess urban multimodal transportation system resilience considering passenger demand and infrastructure supply. Reliab Eng Syst Saf 2023;238.

[52] Jiang J, Zhang D, Meng Q, Liu Y. Regional multimodal logistics network design considering demand uncertainty and CO2 emission reduction target: A system-optimization approach. J Clean Prod 2020;248:119304.

[53] Mejjaouli S, Babiceanu RF. Cold supply chain logistics: System optimization for real-time rerouting transportation solutions. Comput Ind 2018;95:68–80.

[54] Khodakarami M, Mitchell K, Wang X. Modeling maintenance project selection on a multimodal transportation network. Transp Res Rec 2014;2409:1–8.

[55] Wei X, Jia S, Meng Q, Tan KC. Tugboat scheduling for container ports. Transp Res Part E: Logist Trans Rev 2020;142.

[56] Wei X, Meng Q, Lim A, Jia S. Dynamic tugboat scheduling for container ports. Marit Policy

Manage 2021;50:492–514.

[57] Xu X, Zhu Y, Xu M, Deng W, Zuo Y. Vulnerability analysis of the global liner shipping network: From static structure to cascading failure dynamics. Ocean Coast Manag 2022;229:106325.